Research Article

A deeply conserved protease, acylamino acid-releasing enzyme (AARE), acts in plant aging

Sebastian N.W. Hoernstein[1], Buğra Özdemir[1*], Nico van Gessel[1], Alessandra A. Miniera[1], Bruno Rogalla von Bieberstein[1**], Lars Nilges[1], Joana Schweikert Farinha[1***], Ramona Komoll[1****], Stella Glauz[1,] Tim Weckerle[1*****], Friedrich Scherzinger[1******], Marta Rodriguez-Franco[2], Stefanie J. Müller-Schüssele[3], Ralf Reski[1,4]

[1] Plant Biotechnology, Faculty of Biology, University of Freiburg, Schaenzelstrasse 1, 79104 Freiburg, Germany

[2] Cell Biology, Faculty of Biology, University of Freiburg, Schaenzlestrasse 1, 79104 Freiburg, Germany

[3] Molecular Botany, Department of Biology, Technical University of Kaiserslautern, Erwin-Schrödinger-Strasse 70, 67663 Kaiserslautern, Germany

[4] Signalling Research Centres BIOSS and CIBSS, Schaenzlestrasse 18, 79104 Freiburg, Germany

Present address:

* Euro-BioImaging Bio-Hub, EMBL Heidelberg, Meyerhofstraße 1, 69117 Heidelberg, Germany

** Department of Anesthesiology, University Hospital Würzburg, Oberduerrbacher Strasse 6, 97072 Würzburg, Germany

*** Institute for Molecular Biosciences, Goethe University Frankfurt, Max-von-Laue-Str. 9, 60438 Frankfurt, Germany

**** Heraeus Medical GmbH, Philipp-Reis-Straße 8-13. 61273 Wehrheim, Germany

***** Eurofins GeneScan GmbH, Engesserstraße 4, 79108 Freiburg, Germany

****** Centre for Integrative Biodiversity Research (iDiv) Halle-Jena-Leipzig, Puschstrasse 4, 04103 Leipzig, Germany

ORCID-IDs:

Sebastian N.W. Hoernstein: 0000-0002-2095-689X

Buğra Özdemir: 0000-0001-9823-0581

Nico van Gessel: 0000-0002-0606-246X

Alessandra A. Miniera: 0000-0003-1638-5438

Bruno Rogalla von Bieberstein: 0000-0002-9650-4064

Lars Nilges: 0000-0003-0716-7236

Joana Schweikert Farinha: 0000-0002-5602-3901

Ramona Komoll: 0000-0002-3142-0863

Stella Glauz: 0000-0002-2305-4525

Tim Weckerle: 0000-0002-9584-5449

Friedrich Scherzinger: 0000-0001-5825-6621

Marta Rodriguez-Franco: 0000-0003-1183-2075

Stefanie J. Müller-Schüssele: 0000-0003-4061-1175

Ralf Reski: 0000-0002-5496-6711

Corresponding author: Ralf Reski, ralf.reski@biologie.uni-freiburg.de

Key words: ageing, Arabidopsis, Physcomitrella, Physcomitrium, protein oxidation, ROS

Short title: AARE in aging and development

Material distribution footnote. The author responsible for distribution of materials integral to the findings presented in this article in accordance with the policy described in the Instructions for Authors (https://academic.oup.com/plcell) is Ralf Reski (ralf.reski@biologie.uni-freiburg.de).

Abstract

Protein oxidation results from the reaction of amino-acid side chains with reactive oxygen species (ROS) and is partly irreversible. In non-photosynthetic tissues, mitochondria are a main source of ROS, whereas plastids are the major source in photosynthetic tissues. Oxidized proteins suffer from decreased structural integrity and even loss of function, and their accumulation leads to cytotoxic aggregates. In mammals, aggregate formation correlates with aging and is linked to several age-related pathologies. Mammalian proteolytic pathways for clearance of oxidized proteins are under intensive research, while mechanistic insights into this process in plants is scarce. Acylamino acid-releasing (AARE) enzymes are ATP-independent serine proteases, presumably acting on oxidized proteins and operating in a dual exo-/endopeptidase mode. They are found in all domains of life. Here, we investigated AARE enzymes in the moss Physcomitrella and the angiosperm Arabidopsis and identified three homologous nuclear genes in Physcomitrella (PpAARE1-3) and a single nuclear gene in Arabidopsis (AtAARE). Surprisingly, we observed triple localization of the proteins AtAARE and PpAARE1 to plastids, mitochondria and the cytosol *in vivo*, likely conserved across the plant lineage. This represents an ATP-independent possibility for degradation of oxidized proteins in the major source organelles of ROS in plants, which is distinct to mammals. Combinatorial knockout plants and protein interaction analysis revealed specific interactions of the moss AARE isoforms and functions in progressive aging. Analysis of an AtAARE T-DNA mutant further suggests the evolutionary conservation of AARE function in age-related development.

Introduction

Reactive oxygen species (ROS) are byproducts of O_2 metabolism and a common challenge to all aerobic life. ROS play a dual role as they are potentially lethal oxidants but also act as signaling molecules. Therefore, aerobic organisms possess sophisticated redox systems to scavenge and detoxify excess ROS. The major sources of ROS in plant cells are the electron transport chains in mitochondria and plastids, but also in peroxisomes and at the plasma membrane (Tola et al., 2021). Environmental factors such as heat, drought or high light intensities are additional factors for increasing ROS production to detrimental levels. Plants possess a repertoire of detoxifying enzymes such as catalases, superoxide dismutases, ascorbate peroxidases, glutathione peroxidase-like proteins and peroxiredoxins. Electrons for reduction are largely provided *via* non-enzymatic components such as ascorbic acid, glutathione and NADPH (Gratão et al., 2005; Smirnoff, 2000; Sharma et al., 2012; Müller-Schüssele et al., 2020; reviewed in Soares et al., 2019). In addition, a range of heat-shock proteins assist in disaggregation or refolding of damaged proteins (Parsell et al., 1994; Mogk et al., 1999; Queitsch et al., 2000; reviewed in Mogk et al., 2018).

Despite conversion into non-toxic derivatives, the continuous exposure to ROS ultimately leads to oxidation of lipids, DNA, and proteins (Sharma et al., 2012). On the protein level, ROS lead to oxidative modifications such as irreversible cysteine oxidation (Cys-sulfonic acid), advanced glycation end-products (Maillard reaction adducts), derivatives with ROS-generated lipid peroxides (mainly 4-Hydroxyl-(E)-2-nonenal (HNE), Malondialdehyde (MDA), Acrolein), and carbonylation of amino-acid side-chains (mainly Lys, Pro, Arg, Thr) (reviewed in Møller et al., 2007; Ciacka et al., 2020). If not cleared via proteolysis, an excess of oxidized proteins ultimately leads to accumulation of cytotoxic protein aggregates. Interestingly, several studies also indicate a role for ROS-related carbonylation in the transduction of phytohormone signaling (Biswas et al., 2015; Islam et al., 2016; Biswas et al., 2019; reviewed in Tola et al., 2021), although mechanistic insight is lacking.

Plant antioxidant systems and the role of ROS as signaling molecules in abiotic stress responses are intensely studied (Farooq et al., 2019). Yet, factors involved in a plant cell's last line of defense, such as the proteolytic systems for the clearance of irreversibly oxidized proteins, are still underexplored. A class of proteases, namely acylamino acid-releasing enzymes (AARE), are considered to play a role in the degradation of irreversibly oxidized proteins. AARE (also termed APEH/ACPH: acylpeptide hydrolase, AAP: acylaminoacyl peptidase, OPH: oxidized protein hydrolase) are S9 class serine proteases (Rawlings et al., 2018) and appear in multimeric

complexes (Yamauchi et al., 2003; Bartlam et al., 2004). They are conserved across all domains of life as their activity was described in archaea, bacteria, animals and plants (Bartlam et al., 2004; Brunialti et al., 2011; Tsunasawa et al., 1975; Yamauchi et al., 2003). AARE is a bifunctional protease as it cleaves N^α-acetylated amino acids from oligopeptides *via* an exopeptidase mode, but is also able to cleave oxidized proteins *via* an endopeptidase mode (Tsunasawa et al., 1975; Fujino et al., 2000; Shimizu et al., 2003; Nakai et al., 2012; Gogliettino et al., 2014). Yet, it remains unclear if both modes of action are coincident or are modified *via* conformational changes and/or interaction of complex subunits in different organisms.

AARE isoforms from various organisms have been biochemically characterized employing artificial substrates. Their specificities towards synthetic N^α-acetylated amino-acid substrates differ, with archaeal and bacterial enzymes preferring AcLeu and AcPhe substrates (Kiss et al., 2007; Szeltner et al., 2009; Brunialti et al., 2011; Gogliettino et al., 2012) and plant and animal isoforms preferring AcAla, AcMeth or AcGly substrates (Tsunasawa et al., 1975; Scaloni et al., 1992; Yamauchi et al., 2003; Riccio et al., 2015).

Besides substrate specificities, their subcellular localization appears to be conserved among eukaryotes, as human (HsACPH) and Arabidopsis (AtAARE) AARE are reportedly cytosolic enzymes (Shimizu et al., 2003; Nakai et al., 2012). In humans, AARE function has been linked to cancer, neurodegenerative diseases and correlates with proteasomal activity (Scaloni et al., 1992; Yamin et al., 2009; Palmieri et al., 2011; Bergamo et al., 2013). AARE from *Arabidopsis thaliana* (AtAARE) and from cucumber have the reported endo- and exopeptidase functions (Yamauchi et al., 2003), and silencing of AtAARE increased the levels of oxidized proteins (Nakai et al., 2012). AtAARE activity was also detected in plastid stroma fractions, although a fusion with a fluorescent reporter did not co-localize with plastids (Nakai et al., 2012). Suppression of AtAARE *via* RNAi resulted in a slightly enhanced accumulation of oxidized proteins in roots and enhanced electrolyte leakage in leaves, but a further impact on plant physiology was not described (Nakai et al., 2012).

Despite a constantly increasing number of studies on AARE functionality in humans and its association with diseases (Palmieri et al., 2017; Zeng et al., 2017; Marshall et al., 2019, Gogliettino et al., 2021), plant AARE enzymes are far less characterized. Moreover, the complete loss of function of this protease and its impact on physiology has not yet been reported for any organism.

Recently, we identified an AARE homolog from Physcomitrella in a proteomics study on protein arginylation (Hoernstein et al., 2016). Our further analysis revealed altogether three Physcomitrella AARE homologs (PpAARE1-3). In the present study, we analyzed the subcellular localization of those PpAARE isoforms and of their homolog from Arabidopsis (AtAARE). We show that an alternative splicing event is targeting PpAARE1 to plastids, mitochondria and the cytosol. We provide evidence that an alternative translation initiation is sufficient to localize AtAARE to the same three subcellular compartments as PpAARE1. Employing combinatorial moss knockouts and protein co-immunoprecipitation (Co-IP) we show distinct interactions between those three isoforms and their concerted action on life span determination. Likewise, an Arabidopsis AARE loss-of-function mutant exhibits accelerated bolting, as a hallmark of plant aging.

Results

AARE gene family expansion and splice variants

Previously, PpAARE1 (Pp1s619_3V6.1) was identified as the most prominent target for N-terminal arginylation in Physcomitrella (Schuessele et al., 2016; Hoernstein et al., 2016). N-terminal arginylation can mediate poly-ubiquitination *via* the N-degron pathway, thus triggering subsequent proteasomal degradation (Varshavsky, 2011; Varshavsky, 2019). Simultaneously, two homologs (PpAARE2: Pp1s108_134V6.1 and PpAARE3: Pp1s97_68V6.1) were identified, although those were not proven to be arginylation targets (Hoernstein et al., 2016). Meanwhile, a new Physcomitrella genome version with chromosome assembly and updated gene versions was released (Lang et al., 2018). Consequently, the gene accessions used in our present study are PpAARE1 (Pp3c2_30720.1), PpAARE2 (Pp3c12_21080V3.1), and PpAARE3 (Pp3c7_25140V3.1). According to an *OrthoMCL* clustering (Chen et al., 2006) published in Zimmer et al. (2013), all three proteins are homologs of the *Arabidopsis thaliana* acylamino acid-releasing enzyme (AtAARE: AT4G14570, Yamauchi et al., 2003; Nakai et al., 2012). According to publicly available expression data (https://peatmoss.online.uni-marburg.de, Fernandez-Pozo et al., 2020) PpAARE1-3 are expressed in all major Physcomitrella tissues and developmental stages, although at varying levels (Fig. S1a). Except for leaves (phylloids) and spores, PpAARE1 is the most strongly expressed gene of this family (between 4 and 20 times), independent of cultivation conditions. In spores, PpAARE2 is expressed considerably stronger than PpAARE1 and PpAARE3 (Fig. S1a).

Likewise, AtAARE is expressed and translated in basically all major Arabidopsis tissues (Fig. S1b, data utilized from Mergner et al. (2020) and downloaded from http://athena.proteomics.wzw.tum.de/). These data indicate a strong, positive correlation between transcript level and protein abundance consistently across all analyzed tissues (Fig. S1b).

To investigate whether other plant species also possess multiple AARE homologs and whether the PpAARE isoforms are inparalogues, we conducted *BLASTP* searches (Altschul et al., 1997) against protein models from selected species using the protein sequence of AtAARE as a query. Selected species were the alga *Chlamydomonas reinhardtii* (Merchant et al., 2007), the liverwort *Marchantia polymorpha* (Bowman et al., 2017)*,* the peat moss *Sphagnum fallax* (*Sphagnum fallax* v1.1, DOE-JGI, http://phytozome.jgi.doe.gov/)*,* the lycophyte *Selaginella moellendorffii* (Banks et al., 2011), the monocot *Oryza sativa* (Ouyang et al., 2007) and the dicot *Populus trichocarpa* (Tuskan et al., 2006), all available at the Phytozome12 database (https://phytozome.jgi.doe.gov). An additional NCBI BLASTP search against the charophyte *Klebsormidium nitens* proteome (Hori et al., 2014) was performed identifying a single homolog (GAQ80280.1) in this species. We also included proteins of *Funaria hygrometrica* (Kirbis et al., 2020), a close relative to Physcomitrella from the Funariacea family (Ostendorf et al., 2021), in our search. Finally, the AtAARE sequence was again searched against the Physcomitrella (Lang et al., 2018) and Arabidopsis proteomes (Lamesch et al., 2012). Homology of the resulting BLAST hits was confirmed if the reciprocal best BLAST hit against *A. thaliana* was again AtAARE.

In poplar, we identified a single homolog for which three distinct splice variants are annotated (Potri.008G160400.1, Potri.008G160400.2, Potri.008G160400.3). These encode different protein isoforms, but two variants seem to encode non-catalytic proteins. AARE enzymes belong to the family of prolyl-oligopeptidases with a conserved catalytic triad (Ser/Asp/His) in the C-terminal peptidase domain (Rawlings et al., 1991; Polgar, 2002). In splice variant 2 (Fig. S2, Potri.008G160400.2) alternative splicing results in the deletion of the catalytic Asp whereas the whole catalytic triad is lacking in splice variant 3 (Potri.008G160400.3). Hence, we consider these splice variants as non-active and disregard them from further discussion.

In rice, we identified two homologs (LOC_Os10g28020.3, LOC_Os10g28030.1), with an additional splice variant (LOC_Os10g28020.1) at one locus which encodes an N-terminal extension.

In *C. reinhardtii, M. polymorpha*, *S. fallax* and *S. moellendorffii*, we identified a single ortholog each. In *M. polymorpha*, three distinct splice variants are annotated (Mapoly0111s0036.1,

7

Mapoly0111s0036.2, Mapoly0111s0036.3). The latter two are UTR splice variants, thus resulting in the same protein sequence, whereas Mapoly0111s0036.1 encodes an N-terminal extension of 97 amino acids compared to the other two variants. In *F. hygrometrica* we identified three distinct isoforms.

Finally, our BLASTP searches using the latest Physcomitrella protein models (Lang et al., 2018) further confirmed that there are three homologs of AtAARE (Pp3c2_30720V3.1, Pp3c12_21080V3.1, Pp3c7_25140V3.1). Additionally, the BLASTP search using AtAARE as query revealed another hit, Pp3c1_2590V3.1. This gene is composed of a single coding exon and encodes a 131 amino acid protein which harbors the AARE N-terminal domain (PF19283). However, it lacks a catalytic peptidase domain and is hardly expressed across different culture conditions and tissues (Perroud et al., 2018). We also did not find any proteomics evidence across several Physcomitrella MS analyses (Mueller et al., 2014; Fesenko et al., 2015; Fesenko et al., 2016; Hoernstein et al., 2016) for this protein. Therefore, this gene was excluded from further analysis.

We then used phylogenetic reconstruction to investigate the origin of gene duplications within the gene family. As an outgroup, we included the sequences of the well-characterized rat and human AARE isoforms (Tsunasawa et al., 1975; Scaloni et al., 1992) as well as two AARE isoforms of the Antarctic icefish *Chionodraco hamatus* (ChAPEH1-2; Riccio et al., 2015). Physcomitrella and *F. hygrometrica* share three distinct pairs of orthologs hinting at an expansion in the common ancestor of the two species. Our phylogenetic analysis did not resolve AARE subfamilies across kingdoms (Fig. 1a) and we conclude that the gene family expansions observed in rice and in the Funariaceae are lineage-specific events.

In addition, this analysis reveals a closer relationship between PpAARE1 and PpAARE3, which presumably originate from a more recent gene duplication event, compared to PpAARE2. This hypothesis is supported by the fact that the open reading frames (ORFs) of PpAARE1 and PpAARE3 are represented by a single coding exon whereas the ORF of PpAARE2 is split across 17 coding exons, similar to AtAARE (Fig. 1b).

Eleven splice variants are annotated for PpAARE2, but they differ only in the splicing of the UTRs, whereas the translated proteins remain unaffected. The same situation is present for PpAARE3 where nine splice variants are annotated, which only differ in their UTR definitions. In contrast, three splice variants are annotated for PpAARE1 giving rise to two distinct protein isoforms (Fig. 1b; PpAARE1_1, PpAARE1_2). Both splice variants are present in Physcomitrella protonema

(Fig. 1b, c), according to RT-PCR with splice variant-specific primers (Table S2). Alternative splicing in the 5' end results in an N-terminal truncated variant of PpAARE1, whereas the longer non-spliced variant encodes an N-terminal plastid transit peptide according to the predictor *TargetP2.0* (Armenteros et al., 2019; Fig. 1d). A cleavage of the transit peptide at the predicted cleavage site (Ala^{72}-M^{73}, Table S1) of PpAARE1 would release exactly the protein encoded by the short splice variant. In contrast, PpAARE2 and PpAARE3 do not harbor any predicted N-terminal targeting signal. Moreover, PpAARE3 is also lacking the WD40 domain that is present in PpAARE1 and PpAARE2 (Fig. 1d).

We employed *LOCALIZER* (Sperschneider et al., 2017) to check for the presence of an NLS in PpAARE isoforms and found that PpAARE1 and PpAARE3 have a predicted and conserved nuclear localization signal (KRRP), whereas PpAARE2 does not, further supporting our hypothesis that PpAARE1 and PpAARE3 originate from a relatively recent gene duplication event.

With Araport11 (Cheng al., 2017), a new version of the gene model for AtAARE was introduced, exhibiting a longer ORF at the 5' end and decreasing the size of the previously annotated 5' UTR (Fig. 1b). The extension of the original annotated ORF encodes a plastid transit peptide (Fig. 1d) according to *TargetP2.0.* To our knowledge, the longer variant of AtAARE has not yet been investigated, whereas the short variant of AtAARE localizes to the nucleus and the cytosol (Nakai et al., 2012). In agreement with the latter findings, we could predict a nuclear localization signal with *LOCALIZER* (KKKK). Thus, targeting of AtAARE to the cytosol and the nucleus, but also to plastids could be enabled by alternative translation initiation.

Alternative splicing also generates two distinct transcripts for AARE1 in rice (OsAARE1, Table S1), where one variant encodes a potential plastid transit peptide resembling PpAARE1. Poplar AARE (PtAARE) also harbors a plastid transit peptide. Here, an alternative translation start site as observed for AtAARE could be possible as a methionine is also present around the predicted targeting peptide cleavage site. However, we did not find any evidence for alternative translation initiation, such as N$^{\alpha}$-acetylation of the internal methionine. For all other plant species, no N-terminal plastid targeting sequence was predicted. In contrast, in the *C. reinhardtii* CrAARE an N-terminal mitochondrial targeting sequence is predicted (Table S1).
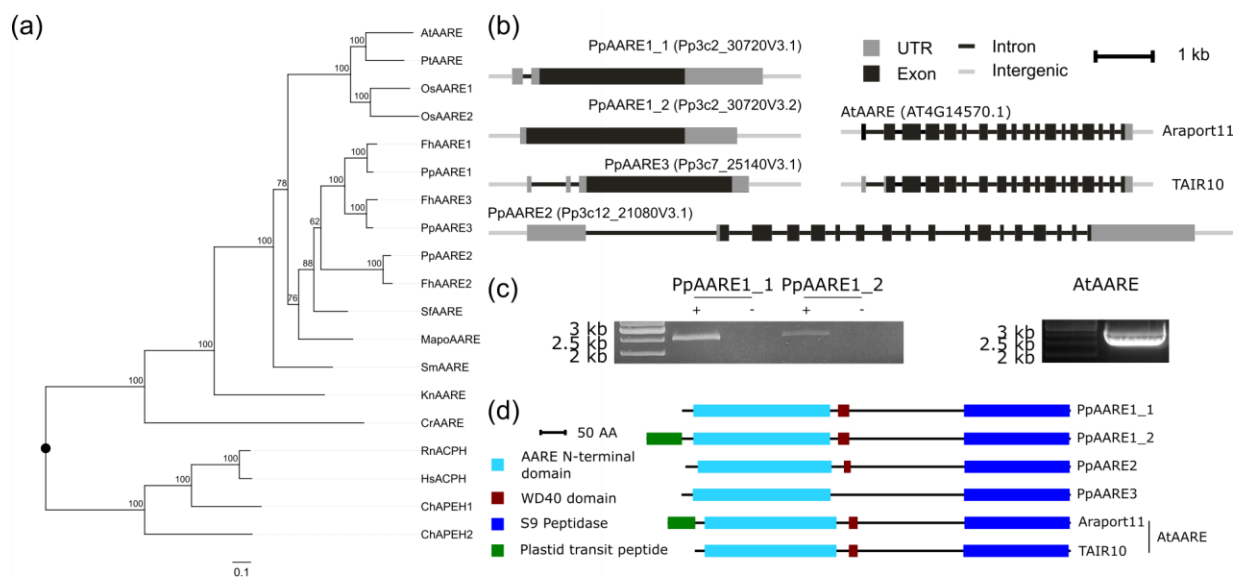
Figure 1 Phylogenetic tree for AARE isoforms from selected organisms, gene structures and proteins domains of *P. patens* and *A. thaliana* AARE isoforms. (a) Maximum likelihood tree based on an alignment of multiple AARE coding sequences. Duplication events in several species appear to be lineage-specific. Node values reflect percentage confidence values based on 1000 bootstrap replicates. Species abbreviations: At: *Arabidopsis thaliana*; Pt: *Populus trichocarpa*; Os: *Oryza sativa*; Pp: *Physcomitrium patens*; Fh: *Funaria hygrometrica*; Sf: *Sphagnum fallax*; Mp: *Marchantia polymorpha*; Sm: *Selaginella moellendorffii*; Kn: *Klebsormidium nitens*; Cr: *Chlamydomonas reinhardtii*; Rn: *Rattus norvegicus*; Hs: *Homo sapiens*; Ch: *Chionodraco hamatus*. (b) Gene structure of PpAARE1-3 and AtAARE. For PpAARE1 two splice variants exist. For AtAARE two different 5' UTR definitions are present (upper: Araport11 (Cheng et al., 2017); lower: TAIR10 (Lamesch et al., 2012)). (c) Left: Both splice variants of PpAARE1 were amplified from cDNA (+: with cDNA template; -: without reverse transcriptase). Expected amplicon size: PpAARE1_1: 2512 bp; PpAA1_2: 2596 bp. Primers were designed to be specific for the splice variants (Table S2). Right: The longer open reading frame of AtAARE was amplified from cDNA. Expected amplicon size: 2457 bp (Table S2). (d) Protein structures showing PFAM-domains for PpAARE1-3 and AtAARE. All isoforms contain AARE N-terminal domain (PF19283) and a catalytic Peptidase S9 domain (PF00326). PpAARE1, PpAARE2 and AtAARE additionally contain a WD40 domain (PF07676). The long splice variant of PpAARE1 and the longer open reading frame of AtAARE encode a predicted N-terminal plastid transit peptide (cTP). AA: amino acid. Cleavable N-terminal sequences were predicted by TargetP2.0 (Armenteros et al., 2019).

PpAARE1 and AtAARE localize to three subcellular compartments

Organellar targeting of AARE has not yet been reported, although Yamauchi et al. (2003) observed AARE activity in plastid-enriched fractions of cucumber. However, plastids, peroxisomes and mitochondria are major hubs of ROS generation (Waszczak et al., 2018), and thus are likely to be organelles with elevated levels of oxidized proteins. Thus, we aimed to investigate whether PpAARE1 and AtAARE would effectively localize to plastids via targeting signals encoded in their N-terminal extensions *in vivo*.

To investigate the subcellular localization of the PpAARE isoforms and of AtAARE, we generated fusion constructs with eGFP for transient expression in Physcomitrella protoplasts. Due to the presence of a predicted plastid targeting peptide for PpAARE1, eGFP was fused in frame to the 3' end of all coding sequences. Since peroxisomes are also ROS-producing organelles, we used *PlantPredPTS1* (Lingner et al., 2011; Reuman et al., 2012) to check for the presence of C-terminal positioned peroxisomal targeting signals. None of the selected AARE isoforms was predicted to localize to peroxisomes (Table S1). Although AtAARE has a C-terminal CKL tripeptide, which is experimentally verified to mediate peroxisomal targeting (Gould et al., 1989; Lingner et al., 2011), the properties of its other C-terminal amino acids most likely prevent peroxisomal targeting. A more recent prediction approach for PTS1-mediated targeting for Arabidopsis proteins (Wang et al., 2017) further supports this conclusion. Peroxisomal targeting can also be mediated *via* N-terminal nona-peptides (R[L|I]x5HL, Reuman, 2004; [R|K][L|V|I]x5[H|Q][L|A], Petriv et al., 2004), but these sequence motifs are also not present within the first 100 aa in any of the selected AARE sequences. In agreement with these predictions eGFP was fused to the 3' end of the coding sequences.

For PpAARE1 three different fusion constructs were assembled. Among these, a fusion of the CDS of the short splice variant (Pp3c2_30720.1) and eGFP was cloned as well as a fusion of the CDS of the longer splice variant (Pp3c2_30720V3.2) and eGFP. Additionally, a fusion of eGFP and the sequence part in which both variants differ (M^1-A^{72}, Pp3c2_30720V3.2) was cloned. This differing sequence part harbors the plastid transit peptide predicted by TargetP2.0. All fusion constructs were expressed under the control of the Physcomitrella Actin5 promoter (Weise et al., 2006; Mueller et al., 2014) in a pMAV4 plasmid backbone as described in Özdemir et al. (2018).

The PpAARE1 isoform derived from the short splicing variant (PpAARE1_1, Fig. 1b) clearly localized to the cytoplasm (Fig. 2). The same localization was observed for PpAARE2 and

PpAARE3 (Fig. 2). Despite a predicted NLS, we could not observe clear nuclear localization, either for PpAARE1 or for PpAARE3.

The isoform encoded by the longer splice variant of PpAARE1 (PpAARE1_2, Fig. 2) localized to plastids and surprisingly also to mitochondria. In contrast to the diffuse cytosolic distribution of PpAARE1, specific foci were observed in plastids. Such foci were not observed for mitochondria. To further investigate whether the N-terminal sequence differing between the two PpAARE1 variants (M^1-A^{72}, Pp3c2_30720V3.2) is sufficient to confer dual targeting, we fused this N-terminal sequence 5' to eGFP and observed again plastid and mitochondrial localization (Fig. 2, PpAARE1_Nt). Full-length PpAARE1 was necessary to localize eGFP to foci within plastids, as the PpAARE1_Nt:eGFP fusion led to a uniform distribution within plastids. However, full-length PpAARE1 was also homogeneously distributed throughout the cytoplasm. This may indicate the presence of interactors that recruit PpAARE1 to specific sites or complexes within the chloroplasts. However, the appearance of those foci may also be an artefact of an impaired import due to the C-terminal eGFP fusion or aggregation within plastids. Further, we conclude that the N-terminal extension of PpAARE1_2 encodes an ambiguous targeting signal for plastid and mitochondrial import as it is capable of localizing the fusion protein simultaneously to plastids and mitochondria.
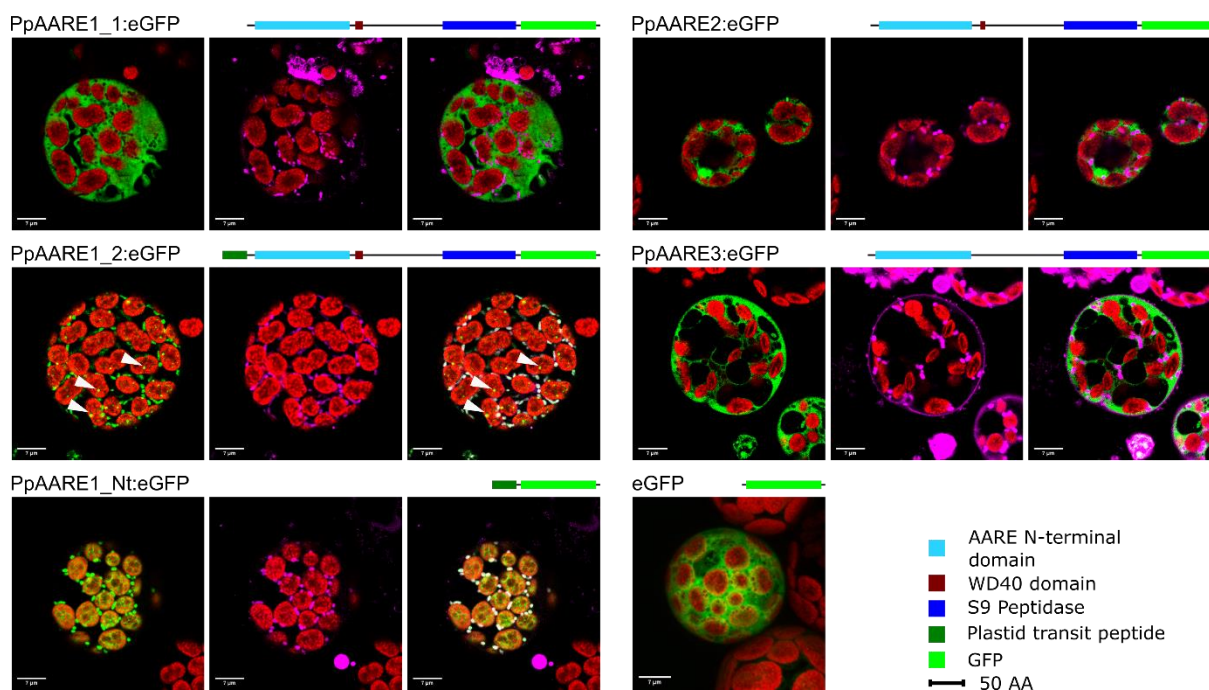

12

Figure 2 Confocal microscopy images showing the localization of PpAARE isoforms with C-terminally fused eGFP in Physcomitrella protoplasts. Fusion proteins with domain structures are depicted. Green: eGFP. Red: chlorophyll. PpAARE1_1, PpAARE2 and PpAARE3 localize to the cytoplasm. PpAARE1_2 localizes to specific foci in plastids (white arrows) and to mitochondria. The N-terminal extension of PpAARE1_2 encoding a predicted plastid transit peptide (PpAARE1_Nt) directs eGFP to plastids and mitochondria. Left image: eGFP (green). Middle image: chlorophyll autofluorescence (red) and MitoTracker™ (purple). Right image: chlorophyll autofluorescence (red), eGFP (green), Mitotracker™ (purple) and co-localization of eGFP and MitoTracker™ (white). Bars = 7 µm.

Based on this data, PpAARE1 is targeted to three different organelles: chloroplasts, mitochondria and the cytosol. This finding was supported by independent evidence; the detection of AARE activity in enriched plastid and mitochondria fractions. Using organelle fractionation as previously described (Lang et al., 2011), we detected AARE activity in plastids, the cytosol, and mitochondria, although to a lesser extent in the latter (Fig. S3).

Simultaneous localization of proteins to plastids and mitochondria can be mediated *via* ambiguous targeting signals which are recognized by both translocation machineries. We evaluated whether ATP2 (Fuss et al., 2013), a tool for the prediction of ambiguous targeting, would recognize PpAARE1 but this was not predicted to be dually targeted. In contrast, AtAARE was predicted to be dually targeted *via* an ambiguous signal by this predictor. Thus, we cloned the analogous three fusion constructs for AtAARE and investigated the subcellular localization of their encoded proteins accordingly.

The AtAARE isoform translated from the shorter ORF (AtAARE, Fig. 1b) localized to the cytoplasm (AtAARE_SV, Fig. 3), as observed for PpAARE1_1 (Fig. 2). This result is partially in agreement with the observation of Nakai et al. (2012) since we could not observe nuclear localization of AtAARE. Using the fusion construct of the longer AtAARE variant, we observed clear dual targeting of the protein to plastids and mitochondria (AtAARE_LV, Fig. 3), as observed for PpAARE1_2 (Fig. 2). Here, the eGFP signal was distributed homogeneously in the chloroplasts, in contrast to the specific plastid foci of PpAARE1:eGFP (Fig. 2).

Next, we cloned only the N-terminal sequence differing between both variants (M^1-A^{55}, longer ORF definition, Fig. 1b) and fused it to eGFP. In order to investigate whether the exact N-terminal difference between the two AtAARE variants would be sufficient for targeting, the M^{56} (same as

13

M^1 in the shorter variant, Fig. 1b), which is the P1 amino acid at the predicted cleavage site, was deleted. Using this construct, the eGFP signal again clearly localized to plastids and mitochondria (AtAARE_Nt, Fig. 3). The signal within plastids was homogeneously distributed, similar to the longer AtAARE variant. Based on these findings we conclude that the N-terminal extension of both long PpAARE and AtAARE variants is sufficient for dual targeting of proteins *in vivo*. Intriguingly, the longer variant of AtAARE localized exclusively to plastids and mitochondria although alternative translation initiation should also be possible in this construct. This is especially interesting as alternative translation initiation is also possible in the longer splice variant of PpAARE1 (PpAARE1_2). But in the latter also the fusion protein localizes exclusively to plastids and mitochondria, which excludes the possibility of an alternative translation initiation, at least in protoplasts. There are numerous transcripts in mammals where translation of an upstream positioned ORF (uORF) suppresses the translation of the downstream main ORF (reviewed in Orr et al., 2020). A similar scenario is conceivable in Physcomitrella based on the present data. However, it remains unclear how and if translation from the internal start codons is controlled. It is also possible that factors controlling alternative translation initiation of AtAARE are absent in Physcomitrella, at least in a spatiotemporal manner, or they might only be triggered at specific physiological situations. According to our data, the translation of the two variants of PpAARE1 is mainly controlled by alternative splicing and not by alternative translation initiation.

In summary, PpAARE1 and AtAARE localize to three subcellular compartments *via* an ambiguous targeting signal, although they were predicted to localize only to plastids. In contrast, PpAARE2 and PpAARE3 localize solely to the cytoplasm.
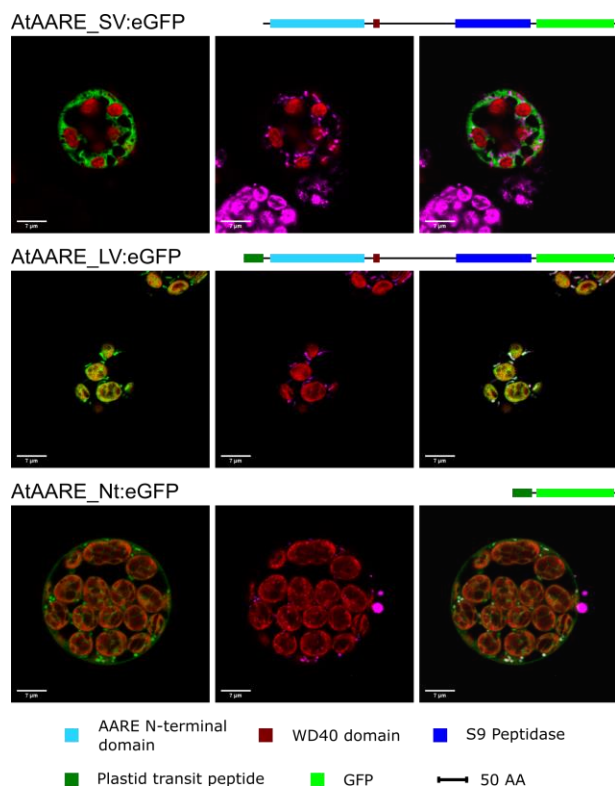
14

Figure 3 Confocal microscopy images of the localization of AtAARE with C-terminal eGFP fusion in Physcomitrella protoplasts. Green: eGFP. Red: chlorophyll autofluorescence. Purple: MitoTracker™ (Thermo Fisher). The short variant (SV) localizes to the cytoplasm. The long variant (LV) localizes to plastids and mitochondria. The N-terminal extension of the long variant of AtAARE localizes to plastids and mitochondria. Left image: eGFP (green). Middle image: chlorophyll autofluorescence (red) and MitoTracker™ (purple). Right image: chlorophyll autofluorescence (red), eGFP (green), MitoTracker™ (purple) and co-localization of eGFP and MitoTracker™ (white). Bars = 7 μm.

Loss of major exopeptidase activity is not linked to phenotypic traits

To gain functional insights, we generated targeted gene knockouts (KOs) of the three PpAARE isoforms in Physcomitrella. PpAARE isoforms 1-3 were knocked out by integrating different selection markers in the genomic loci *via* efficient homologous recombination according to Hohe et al. (2004). For the integration of the respective selection markers, homologous flanks were chosen that delete the full CDS upon integration. Three different selection cassettes (nptII,

hygromycin, zeocin) were chosen (Fig. 4a) to enable the subsequent generation of double and triple KOs. Plants surviving the selection procedure were screened by PCR for the lack of the corresponding CDS and for correct integration of the KO construct (Fig. 4b, d). This resulted in the identification of four independent KO lines for each PpAARE gene. For these independent candidate lines, the number of genomic integrations of the corresponding KO construct was measured via qPCR as described in Noy-Malka et al. (2014), and a line with only a single integration in the genome was detected for each PpAARE KO (Fig. 4c, e). Further, haploidy of all lines was confirmed via flow cytometry (Fig. S4) according to Schween et al. (2003b). For all further experiments only the selected lines with a single integration of the KO construct were used (ΔPpAARE1 #59, ΔPpAARE2 #13, ΔPpAARE3 #17).
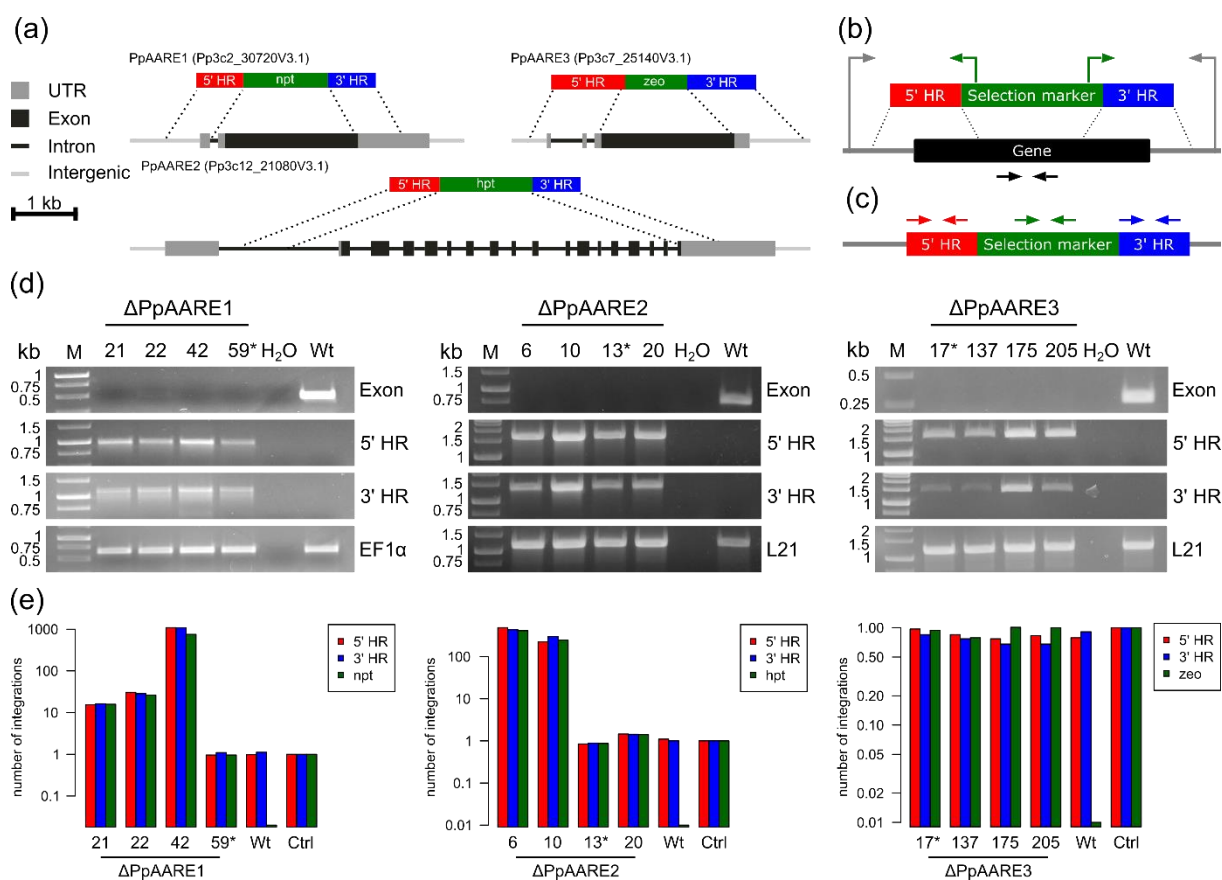

Figure 4 PpAARE gene structures with positioning of the knockout constructs and PCR results. (a) Each isoform was knocked out using a different selection marker. The selection markers confer resistance against G418 (npt), hygromycin (hpt) and zeocin (zeo), respectively.

Homologous regions (HR) were chosen in order to remove the full coding region of the corresponding gene upon integration of the selection marker. (b) PCR scheme showing the primer combinations (arrows) used to validate KOs. One pair each is used to check for the correct positioning of the homologous flanks (5' and 3' HR) at the desired locus (green, gray) and one pair was used to check for the presence/absence of the genomic region (black arrows). (c) Scheme showing primers (arrows) used to determine the copy numbers of the KO construct integrated in the genome via qPCR on genomic DNA. Primers are listed in Table S2 and Table S4. (d) PCR validation of KOs for PpAARE1, PpAARE2 and PpAARE3 performed on genomic DNA. Expected amplicon sizes for PpAARE1: Exon: 497 bp; 5' HR: 983 bp; 3' HR: 1128 bp. Expected amplicon sizes for PpAARE2: Exon: 768 bp; 5' HR: 1678 bp; 3' HR: 1309 bp. Expected amplicon sizes for PpAARE3: Exon: 273 bp; 5' HR: 1631 bp; 3' HR: 1486 bp. EF1α and L21 are reference genes. Expected amplicon sizes: EF1α: 660 bp; L21: 1173 bp. Stars mark lines which have one single integration of the KO construct. (e) Copy number count of the respective KO constructs for each validated KO line determined via qPCR. Ctrl: Single integration control for each employed selection marker.

In the single KO mutants of each AARE isoform we did not observe any impact on growth or gametophore development, as neither protonema nor gametophores showed apparent phenotypical deviations from WT when cultivated under standard laboratory conditions (Fig. 5a). This indicates that the function of each single PpAARE isoform is not required for growth and development under standard laboratory conditions, possibly because of functional redundancy.

AARE exopeptidase activity is typically measured on substrates with N$^\alpha$-acetylated amino acids, such as AcAla or AcMet coupled to a measurable reporter, such as para-nitro-anilide (pNA) or 7-amido-4-methylcoumarin (AMC). Among these, AcAla-pNA has been tested as substrate for several eukaryotic AARE isoforms, including AtAARE (Scaloni et al., 1992; Yamauchi et al., 2003; Gogliettino et al., 2014). We inspected the overall AARE activity of crude extracts in the PpAARE KOs compared to WT with AcAla-pNA as substrate and additionally included AcLeu-pNA as complementary substrate. We did this because AcLeu substrates were used to characterize archaeal, bacterial, and several eukaryotic AAREs (Tsunasawa et al., 1975; Kiss et al., 2007; Szeltner et al., 2009; Brunialti et al., 2011; Gogliettino et al., 2012; Gogliettino et al., 2014).

Intriguingly, only the knockout of PpAARE1 lead to a significant decrease in overall AARE activity towards AcAla-pNA in protonema and in gametophores. In contrast, the knockout of PpAARE2

and PpAARE3, respectively, did not have a significant impact on overall AARE activity (Fig. 5b). This observation was consistently made in all identified single knockout lines (Fig. S5a-c).

In both tissues, the juvenile protonemata and the adult gametophores, we detected only weak activity on AcLeu-pNA in all Physcomitrella genotypes (Fig. 5b). Nevertheless, the KO of PpAARE1 further reduced this activity, at least in protonema. As we detected only minor PpAARE exopeptidase activity on AcLeu-substrates, this substrate was excluded from further tests.
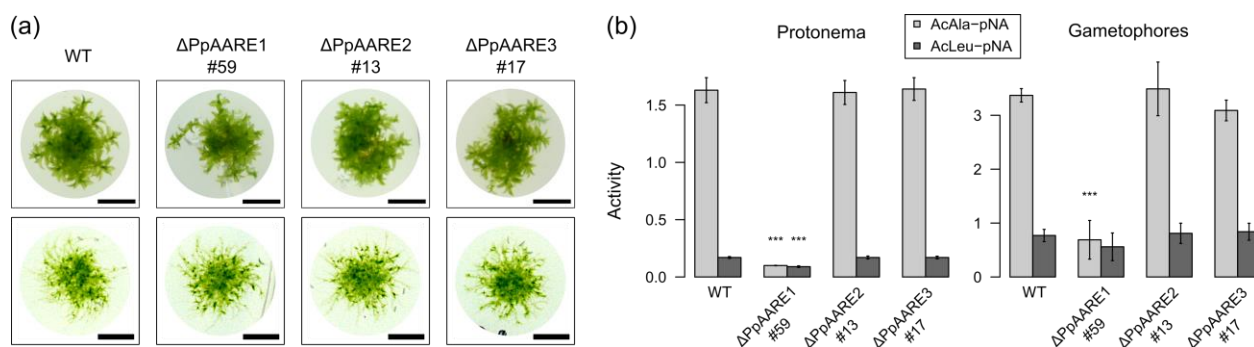
Figure 5 Phenotype and AARE activity in protonema and gametophores of Physcomitrella WT and AARE KOs. (a) Gametophores (upper panel) and protonema (lower panel) develop normally and do not show any obvious deviation. Bar = 5 mm. (b) Mean AARE activity in Physcomitrella protonema and gametophores of three biological replicates with standard deviations. Significance levels are based on a one-way Anova and subsequent post-hoc test (***: $p < 0.001$) and indicate differences compared to WT. Activity on AcAla-pNA is significantly reduced in protonema and in 13-week-old gametophores of ΔPpAARE1 compared to WT and to the other knockout mutants. Gametophores were cultivated in hydroponic cultures on glass rings. In protonema, the activity on AcLeu-pNA is also significantly reduced compared to all other plants.

In summary, our data on AARE exopeptidase activity indicate that loss of PpAARE1, which is localized in three organelles, is not compensated by the other two isoforms, which are exclusively cytosolic. We consistently found PpAARE1 exopeptidase activity in protonemata and in gametophores grown under normal conditions. However, loss of PpAARE1 activity evidently did not alter plant growth and development under these conditions. Consequently, PpAARE1 is the dominant isoform responsible for the main exopeptidase activity in Physcomitrella protonema and

18

gametophores. However, we cannot rule out that the cytosolic PpAARE2 and PpAARE3 can compensate for the lack of each other. Compensation of loss-of-function mutants is repeatedly observed in different model organisms such as mouse, Arabidopsis, and zebra fish (reviewed in El-Brolosy & Stainier, 2017). To gain deeper functional insights, we generated subsequent double and triple knockout mutants (doKOs, triKOs).

Double null mutants of PpAARE1/2 exhibit accelerated aging

We generated all possible combinations for double knockouts using ΔPpAARE1 #59 and ΔPpAARE3 #17 as parental lines. As for the single KOs, plants surviving the selection procedure were checked by PCR (Fig. 4b, c). In the following, the names of the doKO and triKO mutants indicate the order of the knockouts (beginning with the index of the parental line). We identified four independent lines for ΔPpAARE1/3 and ΔPpAARE3/2 and three independent lines for ΔPpAARE1/2 (Fig. 6a). Again, the copy number of genomic integrations of the respective KO construct was determined via qPCR. For each doKO at least one line with a single integration was detected (Fig. 6b-d). The overall AARE activity was significantly decreased in all doKO mutants lacking PpAARE1 (ΔPpAARE1/3, ΔPpAARE1/2). In three of the four ΔPpAARE3/2 mutants, the overall activity was slightly increased (Fig. S5d-f). ΔPpAARE3/2 #43 showed no difference to WT at the activity level across different experiments (Fig. S5f, Fig. 7f) and was chosen for further experiments.

Additionally, PpAARE triKOs were generated using ΔPpAARE1/3 #6 as parental line. Here, five independent mutants were identified (Fig. 6e), three of them with a single integration of the third KO construct in the genome (Fig. 6f). Haploidy of all mutants was confirmed by flow cytometry (Fig. S6, S7).
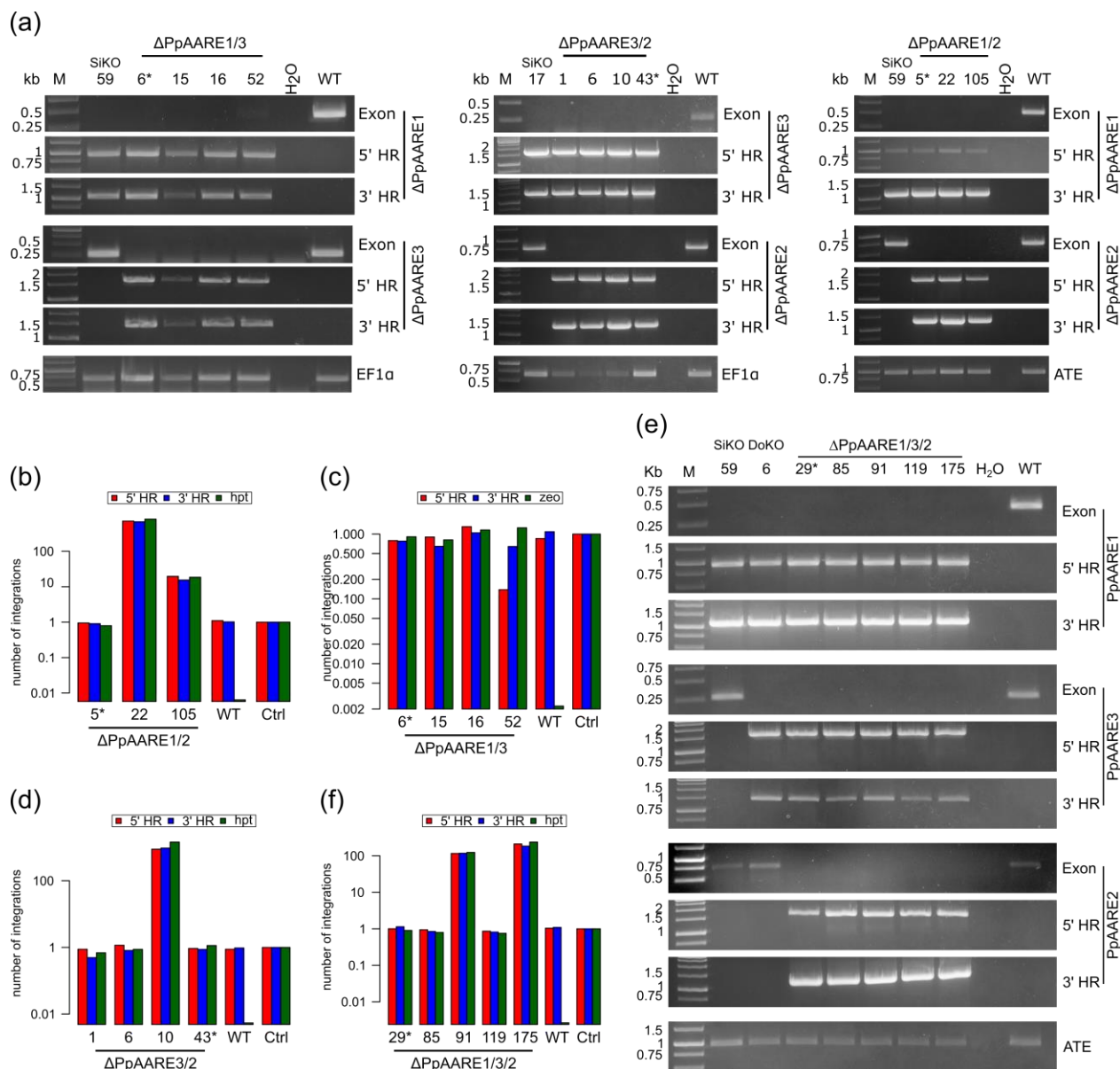
Figure 6 Identification of PpAARE double and triple KO mutants. (a) PCR (genomic DNA) based identification of ΔPpAARE1/3, ΔPpAARE3/2 and ΔPpAARE1/2 lines. SiKO indicate the single KO line employed as parental line. Primers used were the same as applied before (Fig. 4). Stars indicate lines with only a single genomic integration of the KO construct selected for further experiments. Copy numbers of the integrated KO constructs were determined via qPCR (b-d, f). (e) PCR (genomic DNA) based identification of ΔPpAARE1/3/2 triple KO lines. DoKO indicates the parental line ΔPpAARE1/3. ATE: reference gene, expected amplicon size: 970 bp (Table S2).

20

To test for developmental or growth phenotypes, we analyzed colony growth of protonema cultivated for 10 weeks in suspension. We did not observe differences between WT and the different KO lines when spotted on solid medium (Fig. 7a, b). In contrast, gametophores were already present in ΔPpAARE1/2 and ΔPpAARE1/3/2, but not to this extent in WT and the other lines (Fig. 7a). This indicates premature gametophore induction in lines with a doKO of PpAARE1/2, which is linked to cytokinin (Reski and Abel, 1985) and sugar availability (Lorenz et al., 2003). This effect was even more pronounced when suspensions of protonema cultivated for 5 months was used. Here, gametophores of ΔPpAARE1/2 and ΔPpAARE1/3/2 were bigger, and colonies denser (Fig. 7c), indicating accelerated gametophore induction. In this culture, significant differences in initial colony expansion were also observable (Fig. 7d). Whereas ΔPpAARE1/3 showed a significant reduction in colony growth compared to WT, no significant differences were observed for the other mutants. Intriguingly, gametophores of ΔPpAARE1/2 and ΔPpAARE1/3/2 were severely stunted (Fig. 7e) compared to WT, ΔPpAARE1/3, and ΔPpAARE3/2. Likewise, gametophore colonies of ΔPpAARE1/2 and ΔPpAARE1/3/2 were smaller and denser.

The exopeptidase activity profile of gametophores (Fig. 7f) was in agreement with the observations from protonema suspension cultures (Fig. S5), where only loss of PpAARE1 led to significantly reduced activity. Subsequently, we analyzed the levels of protein oxidation in gametophores. In this assay, protein carbonyl groups derived from oxidation are derivatized with 2,4-dinitrophenylhydrazine (DNPH) to 2,4-dinitrophenylhydrazone (DNP). This irreversible modification is then recognized on Western blots by a primary anti-DNP antibody. Since DNPH can also react with oxidation states of cysteine side chains (Dalle-Donne et al., 2009), we regard this assay as analysis of general protein oxidation and not only of protein carbonylation. In this assay, the doKO of PpAARE1 and PpAARE2 had the strongest effect on the total amount of oxidized proteins (Fig. 7g, Fig. S8). In contrast, the KO of PpAARE3 did not have a pronounced effect on the level of oxidized proteins. Taken together, our results reveal that AARE exopeptidase activity is not indicative of the level of oxidized proteins in Physcomitrella.
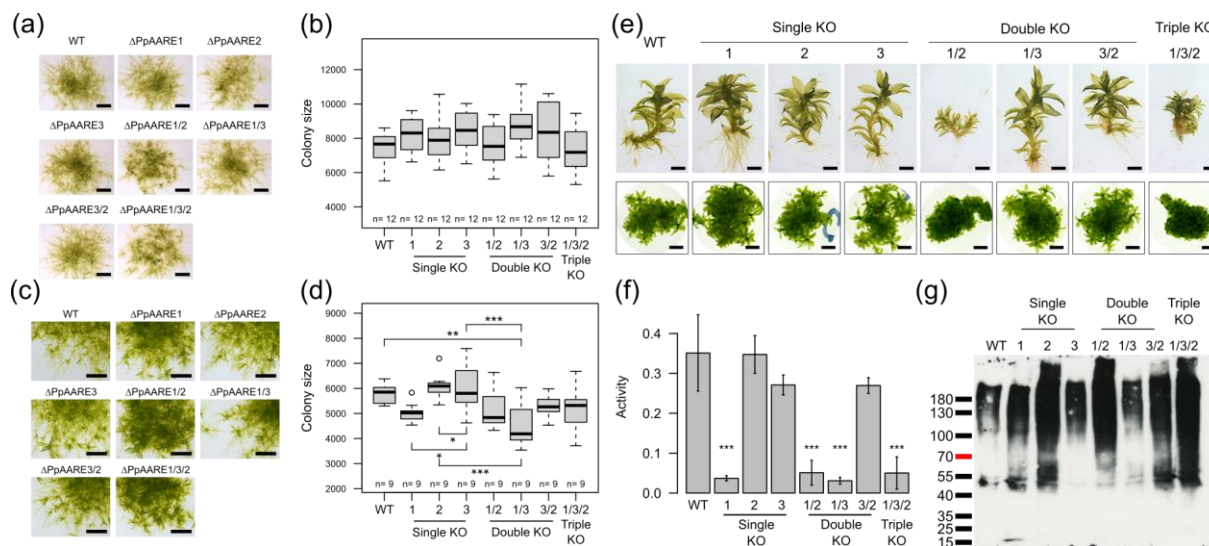
Figure 7 Comparison of phenotypes, AARE activity and level of protein oxidation between Physcomitrella WT and all types of KO mutants. (a) Protonema colonies grown on KnopME with 0.02% glucose spotted from $2^{1}/_{2}$-month-old suspension culture (440 mg DW/L). Bar = 1 mm. Images were taken 9 days after spotting. (b) Box plot showing the distribution of colony areas (n=12 colonies per boxplot; colony images taken 7 days after spotting). No significant difference of colony areas between WT and the KOs were observed (tested via one-way Anova). (c). Protonema colonies grown on KnopME with 0.02% glucose spotted from 5-month-old suspension culture (440 mg DW/L). Images were taken 16 days after spotting. Bar = 0.5 mm. Colonies of ∆PpAARE1/2 and ∆PpAARE1/3/2 have bigger gametophores indicating premature gametophore induction. Additional full colony-size images are available in Fig. S9. (d) Box plot showing the distribution of the colony areas 6 days after spotting (n=9 colonies per boxplot). (e) Phenotypes of gametophores of WT and the different KOs cultivated on KnopME for 4 months. All colonies were grown on the same plate. Upper panel: Bar = 0.5 mm; lower panel: Bar = 2mm. (f) Mean AARE exopeptidase activity on AcAla-pNA in gametophores. Depicted is the mean of three colonies per line with standard deviations. All colonies were cultivated on the same plate. Significance levels indicate differences compared to WT. (g) Levels of protein oxidation in gametophores of WT and the different KOs. The analysis was repeated three times and a Coomassie-stained loading control is available in Fig. S8. Gametophore colonies (e, f, d) were started by transplanting tissue between plates (KnopME). Significance levels in activity assays and boxplots are based on a one-way Anova and subsequent post-hoc test (*: $p<0.05$; **: $p<0.01$; ***: $p<0.001$). Detection of protein oxidation was performed with the OxyBlot[TM] *Protein Oxidation Detection Kit* (Merck). Colony areas were measured with *ImageJ*. Quantitative values represent white pixels counted from binarized colony images with *ImageJ*.

Another remarkable difference between WT and mutants with a double KO of PpAARE1/2 was observable in older plants. After 5 months of cultivation, ΔPpAARE1/2 and ΔPpAARE1/3/2 were only viable at the tip of the gametophores (Fig. 8, plate 1), whilst most of the colony was already dead. In contrast, gametophores of WT and the other KOs were fully viable. After 8 months, ΔPpAARE1/2 and ΔPpAARE1/3/2 were already dead, in contrast to WT and the respective parental lines, which only showed some dead gametophores (Fig. 8, plate 2). In summary, mutants with a double KO of PpAARE1/2 exhibit accelerated developmental transition from protonema to gametophore (Fig. 7a, c), while size and life span of gametophores is strikingly reduced. In contrast, these effects are not visible in ΔPpAARE1/3. Therefore, we conclude that these aging phenotypes correlate with the levels of oxidized proteins but not with measurable AARE exopeptidase activity.
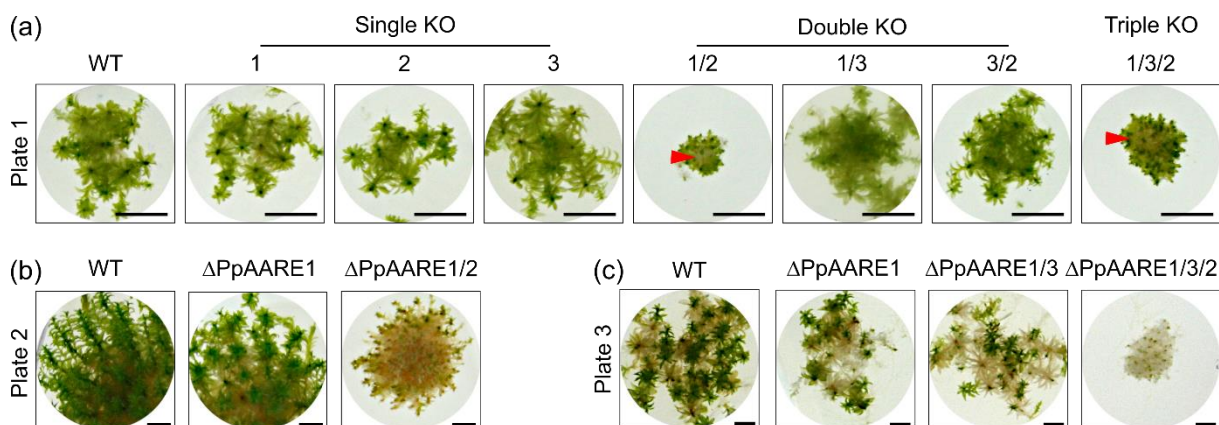

Figure 8 Physcomitrella gametophore colonies of varying age. (a) Colonies of all representative knockout mutants after 5 months on solid medium (KnopME). Bar = 5mm. Gametophores of ΔPpAARE1/2 and ΔPpAARE1/3/2 are only viable at the tip, whereas plant material at the base (red arrow) is dead. (b) Colonies after 8 months on solid medium. ΔPpAARE1 is the parental line for ΔPpAARE1/2. Gametophores of WT and ΔPpAARE1 are still viable whereas ΔPpAARE1/2 gametophores are mostly dead. Bar = 2 mm. (c) Colonies after 8 months on solid medium. ΔPpAARE1 is the parental line for ΔPpAARE1/3 and ΔPpAARE1/3 is the parental line for ΔPpAARE1/3/2. Colonies of WT, ΔPpAARE1 and ΔPpAARE1/3 still have viable gametophores, whereas ΔPpAARE1/3/2 gametophores are dead. Bar = 2 mm.

Distinct *in-vivo* interactions of PpAARE isoforms

In different organisms, AARE isoforms form different types of homomeric complexes such as dimers (Bartlam et al., 2004), tetramers (Yamauchi et al., 2003), or hexamers (Szeltner et al., 2009). Thus, we analyzed whether the PpAARE isoforms can interact with each other, indicating heteromeric AARE complexes in Physcomitrella. In a previous proteomics study, all three isoforms were identified, although the protein modification used for pulldown (N-terminal arginylation) was only identified on PpAARE1 (Hoernstein et al., 2016). This finding stimulated two hypotheses: First, PpAARE2 and PpAARE3 are also targets for Nt-arginylation, but peptides modified accordingly were not identified for these isoforms. Second, the isoforms interact in complexes which were pulled down due to the Nt-arginylation of PpAARE1. To analyze the potential interaction of the isoforms *in vivo* we generated Citrine fusion lines for each isoform *via* in-frame tagging at the native locus using homologous recombination (knock-in, Fig. 9a). The original stop codons of the respective PpAARE CDS were deleted. The Citrine-tag was intended to enable two different types of analysis: First, it should enable further *in-vivo* monitoring of PpAARE isoforms expressed from the native promoter, and second, it is a valid tag for co-immunoprecipitation via commercially available trap-beads.

Plants surviving the selection after transfection were screened by PCR and haploidy was confirmed by flow cytometry (Fig. S10). In plants with a detectable fusion transcript (Fig. S11a-c) the presence of the target protein was checked *via* IP and subsequent MS analysis. For PpAARE3:Citrine lines, we detected transcripts in only one line and obtained only insufficient coverage and intensity at the MS across several performed Co-IPs. Thus, these fusion lines were excluded from further analysis. The co-precipitation of other PpAARE isoforms with the respective bait isoforms was observed (Fig. S11d-e) confirming the MS-Data of Hoernstein et al. (2016). All plants harboring the Citrine fusion were phenotypically inconspicuous (Fig. S11f). Although the fusion proteins were detected in two independent lines for each of the two isoforms (PpAARE1, PpAARE2), we could not observe any Citrine signal within Physcomitrella protonemata or gametophores, most likely due to the low abundance of the PpAARE isoforms. Nevertheless, MS intensities and sequence coverage enabled quantitative Co-IP to investigate the potential interaction of the isoforms.

When targeting PpAARE1:Citrine, both other isoforms, PpAARE2 and PpAARE3, appeared as significant interacting partners (Fig. 9b, p < 0.01, FDR = 0.01). In a reciprocal Co-IP targeting PpAARE2:Citrine only, PpAARE1 appeared as significant interacting partner. PpAARE3 was not

detected in this pulldown. Although lacking a reciprocal IP targeting PpAARE3:Citrine, the present data allows us to conclude that PpAARE1 interacts with PpAARE2 and PpAARE3, whereas PpAARE2 apparently only interacts with PpAARE1. Consequently, there are distinct interactions of PpAARE1 with PpAARE2 and PpAARE3 *in vivo*, possibly resulting in cytosolic heteromeric AARE complexes in Physcomitrella.
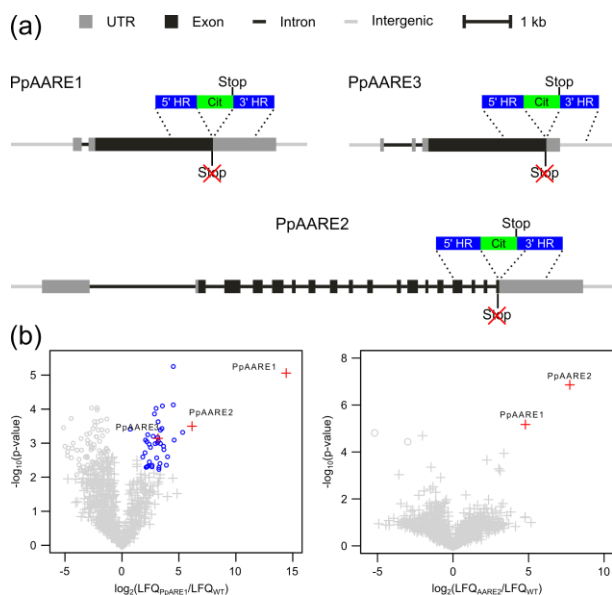

Figure 9 Reciprocal co-immunoprecipitation (Co-IP) with Citrine-tagged PpAARE isoforms. (a) Tagging of PpAARE isoforms was realized by in-frame fusion with a linker-Citrine CDS at the respective native locus via homologous recombination. Original stop codons were deleted. (b) Volcano plots showing the result of the Co-IP´s against each of the PpAARE:Citrine fusion proteins. Left panel: Pulldown of PpAARE1:Citrine. Right panel: Pulldown of PpAARE2:Citrine. Co-IP was performed with GFP-Trap Magnetic Particles M-270 (Chromotek) and protonema from suspension culture. Log$_2$ ratios of normalized label-free quantitation values (LFQ) are plotted against –log$_{10}$ of adjusted p-values. Proteins significantly enriched in the Citrine tagged pulldown are shown in blue circles (p < 0.01, FDR = 0.01). Significantly enriched PpAARE isoforms are depicted as red crosses.

AtAARE affects bolting time

In Physcomitrella, three AARE genes exist, and the concerted action and interaction of the translated isoforms are likely determinants of plant aging. To analyze if this is an evolutionary conserved function, we analyzed the situation in Arabidopsis. Here, only a single AARE gene is present according to our blast searches and phylogenetic analysis (Fig. 1). It was reported that silencing of AtAARE leads to an accumulation of oxidized proteins, whereas overexpression did not affect the level of protein oxidation (Nakai et al., 2012). To gain deeper insights, we screened for available Arabidopsis T-DNA mutants.

Two T-DNA insertion lines (SALK_071125 and GK-456A10) were identified using the public T-DNA Express database at the SIGnAL website (http://signal.salk.edu). SALK_071125 (s68) has a T-DNA insertion in an intron at the predicted 5´UTR of the AtAARE gene model, whereas the T-DNA insertion in GK-456A10 (GK) maps to an intron in the region encoding the catalytic domain (Fig. 10a). Homozygous populations of GK-456A410 containing the T-DNA insertion were identified by their resistance to sulfadiazine and their genotype was confirmed by PCR. In the case of the Salk line (s68), homozygous plants had lost their resistance to kanamycin, but their genotype could be confirmed by PCR. Homozygous plants of both genotypes were back-crossed with Col-0, and brought to homozygosis for subsequent experiments. Primers for screening and validation of both T-DNA lines (GK and s68) are listed in Table S6. Additionally, we analyzed remaining gene expression in both T-DNA lines via RT-PCR. The transcript of AtAARE was still detectable in both lines (Fig. 10a), although very reduced in s68, while the protein was not detectable *via* Western blot (Fig. 10b). Surprisingly, the WT signal of AtAARE was detected at around 100 kDa. The estimated molecular weight is approximately 84 kDa (90 kDa for the longer ORF variant without cleavage of the plastid targeting peptide). This may indicate the presence of yet unknown posttranslational modifications.

The exopeptidase activity on AcAla-pNA was significantly reduced in both independent T-DNA insertion mutants. In contrast, the activity on AcLeu-pNA did not change significantly, although a slight reduction was observed in the GK line (Fig. 10c). Thus, in agreement with Western blot and activity data, the remaining transcripts detected *via* RT-PCR (Fig. 10a) do not seem to be translated to fully functional proteins. The activity on AcLeu-pNA was also comparably lower than that observed for Physcomitrella. At first sight, we did not observe any impact on growth or development in the analyzed T-DNA lines (Fig. 10d, Fig. S13). Based on this characterization, we concentrated our subsequent experiments on T-DNA mutant line s68.
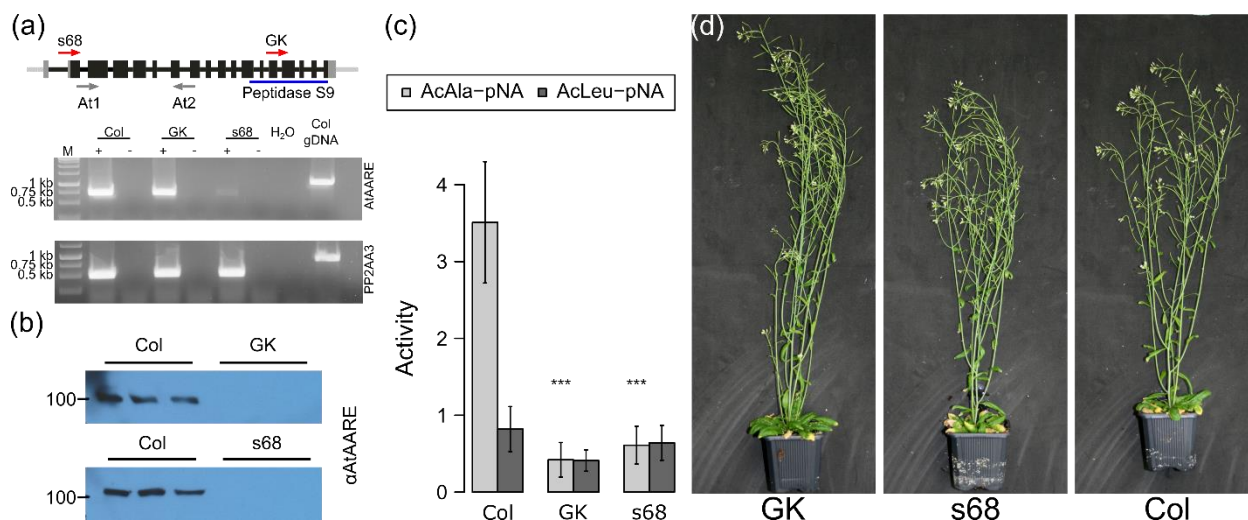
Figure 10 Molecular and phenotypical characterization of two *A. thaliana* T-DNA mutant lines. (a) Structure of the AtAARE gene and positions of T-DNA insertions (red arrows indicate positions of T-DNA insertion, s68 (SALK_071125) and GK (GK-456A10)) and primers (At1, At2) used for RT-PCR (below). Transcription analysis of AtAARE was performed by RT-PCR in WT (Col), s68, and GK plants. Negative controls without reverse transcriptase (-), a water control (H₂O) and genomic DNA control (gDNA) are indicated. Expected amplicon sizes: AtAARE: cDNA 739 bp, gDNA: 1204 bp; PP2AA3 (reference gene): cDNA: 517 bp, gDNA: 911 bp. Primers are listed in Table S6. (b) Western blot analysis on extracts of the two T-DNA mutants and WT probed with a polyclonal @AARE antibody. In both T-DNA lines AtAARE is not detectable. (c) Mean exopeptidase activity in *A. thaliana* extracts on AcAla-pNA and AcLeu-pNA with standard deviations (n = 3 biological replicates). Significance levels are based on one-way Anova and subsequent post-hoc test (***: p<0.001) and indicate differences compared to WT (Col). (d) Plants were grown under short day conditions (8h light/16h dark) for 4 weeks and then transferred to long day conditions for another 3 weeks (16h light/8h dark).

The most striking feature reported in Nakai et al. (2012) was the increase of oxidized proteins in AtAARE-silenced plants. To corroborate this, we investigated levels of oxidized proteins in the T-DNA mutant (s68) in comparison to WT (Col-0). We analyzed plants cultivated under short day conditions to delay bolting (Levey & Wingler, 2005). In both genotypes, the distribution of oxidized proteins was different to Physcomitrella gametophores and protonemata (Fig. 11a). Using the same extraction protocol, oxidized proteins in Arabidopsis were mainly detectable at lower molecular weight, whereas in Physcomitrella mainly signals at higher molecular weight were

27

observed (Fig. 7g). Despite these differences between Physcomitrella and Arabidopsis, the level of protein oxidation was apparently higher in the Arabidopsis mutant (s68) than in WT (Col, Fig 11a).

Johansson et al. (2004) analyzed the levels of oxidized proteins during the Arabidopsis life cycle and observed an accumulation of oxidized proteins during vegetative growth, which was depleted at the transition to bolting. It was not clear from this study, whether the level of oxidized proteins represents a signal for shoot induction, or if the reset of protein oxidation at the bolting transition is a side-effect of enhanced protein turnover during this process. To address this question we assessed the bolting behavior of WT and mutant plants. Effectively, bolting in mutant plants differed significantly from WT. Bolting started in WT at 24±1 rosette leaves, whereas it started at 21±2 rosette leaves in the mutant (Fig. 11b). Consequently, this earlier shoot induction in the mutant correlates with enhanced levels of oxidized proteins, which may be a signal for the transition from vegetative to generative phase.
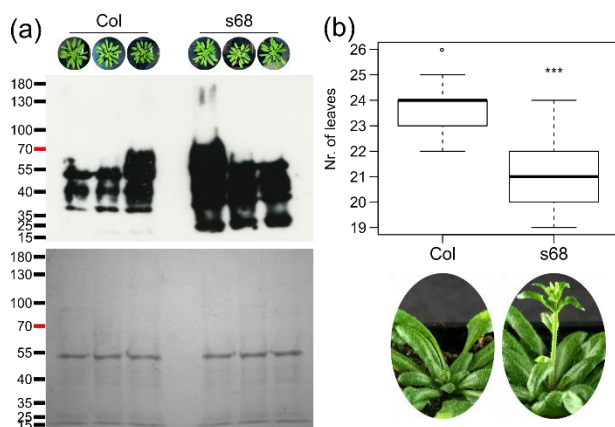

Figure 11 Levels of oxidized proteins in Arabidopsis and bolting phenotype analyses. (a) Detection of protein oxidation in WT (Col) and ΔAtAARE mutant (s68). From three independent plants one exterior rosette leaf was taken after cultivation for 8 weeks in short-day conditions (8h light/16h dark). Protein loading control by Coomassie staining is depicted below. (b) Boxplot of the bolting analysis of WT (Col, n = 14) and AtAARE mutant plants (s68, n=13). Significance level is based on one-way Anova and subsequent post-hoc test (***: p<0.001). Exemplary plants (45-day-old plants grown in long-day conditions, 16h light/8h dark) are depicted below the boxplot.

Discussion

A universal definition of aging is difficult due to strongly differing characteristics between and within the domains of life. In humans, the term aging is inherently linked to degenerative diseases whereas plant aging is considered as the progression of developmental transitions from seeds to senescence. However, a common feature of aging in all living beings is the execution of a predestined genetic program that controls growth, development and maturation. In turn, the progression of this genetic program is functionally dependent on the metabolic state and linked to environmental factors. Among the molecules responsible for the conduction and progression of these processes are ROS. The theory of ROS-involvement in aging and diseases such as cancer was postulated by Harman (1956) and was extended by considering mitochondria as central sources (Harman, 1972). In humans, mitochondrial malfunction in line with increased ROS levels is a central determinant of aging and associated pathologies (Giorgi et al., 2018). In plants, mitochondrial ROS increase during aging of seeds (Mao et al., 2018) and are considered to be major determinants of germination capacity (Ratajczak et al., 2019). In photosynthetic tissues, chloroplasts are the major source of ROS, and their formation increases during aging (Munné-Bosch & Alegre, 2002; Noctor et al., 2002; Foyer et al., 2003). Plants cannot escape from stress situations that increase ROS production to detrimental levels, such as heat, drought, or strong light intensities. Despite several layers of ROS defense, oxidized proteins likely constitute the major share of modified molecules. Consequently, protein oxidation and resulting aggregate deposition are concomitant of aging (López-Otín et al., 2013). The degradation of artificially oxidized proteins by AARE enzymes has been demonstrated repeatedly, and silencing of AtAARE in turn increased the levels of oxidized proteins (Fujino et al., 2000; Shimizu et al., 2003; Nakai et al., 2012; Gogliettino et al., 2014). However, a contribution of AARE to the process of aging remained elusive, although several studies associate AARE-function to age-related diseases (Senthilkumar et al., 2001; Santhoshkumar et al., 2015; Palmieri et al., 2017). Additionally, attention is paid to human AARE for potential anti-cancer treatments (Palumbo et al., 2016; Tangri et al., 2021).

Here, we identify three genes encoding AARE isoforms in Physcomitrella. This is a gene family expansion that is seemingly an outstanding feature of the moss family Funariaceae, as most organisms we analyzed contain only a single AARE gene, and only a few have two (Fig. 1). We analyzed those three AARE isoforms in Physcomitrella (PpAARE1-3) and compared selected features to the single isoform in Arabidopsis (AtAARE). Our data reveal specific functions in life span determination and age-related developmental transitions.

Surprisingly, we found triple localization of AtAARE and PpAARE1 to plastids, mitochondria and the cytosol *in vivo*, suggesting a functional role for AARE in these three cellular compartments. In Physcomitrella, the triple localization is mediated *via* alternative splice variants and in Arabidopsis likely *via* alternative translation initiation. Although there have been occasional indications of AtAARE being associated to plastids (Yamauchi et al., 2003; Nakai et al., 2012), there was no clear evidence for organellar targeting of this protease until now. It is remarkable, that the triple localization of this protease is evolutionary conserved between Arabidopsis and Physcomitrella, although executed *via* different molecular mechanisms.

AARE exopeptidase activity was observed in plastid-enriched fractions of cucumber (Yamauchi et al., 2003) and this finding is supported by the identification of AtAARE in plastid-enriched fractions of Arabidopsis *via* MS (Zybailov et al., 2008). In contrast, PpAARE1 was not identified in plastid proteome analyses in Physcomitrella (Mueller et al., 2014; Fesenko et al., 2016). Nevertheless, we observed AARE exopeptidase activity in enriched plastid fractions of this moss (Fig. S3). Plastids are a major source of ROS in photosynthetic tissues exposed to light, whereas mitochondria are the major source of ROS in non-photosynthetic tissues or in the dark (Maxwell et al., 1999; Møller 2001; Noctor et al., 2002, Foyer et al., 2003). Until now, it remained unresolved how plants deplete oxidized protein content from plastids and mitochondria. In yeast and mammals, the ATP-dependent LON and AAA proteases are involved in clearance of misfolded and oxidized mitochondrial proteins. Intriguingly, mutants of plant homologs of LON proteases did not show clear effects in the levels of oxidized proteins, but AAA-type FTSH proteases may play a role (reviewed in Smakowska et al., 2014). However, under stress conditions, such as heat, drought or high light, photosynthesis is compromised due to the destruction of core components of photosystem II (Al-Khatib, & Paulsen, 1989; Wang et al., 2018). Accordingly, oxidative stress impairs mitochondrial respiration (Sweetlove et al., 2002) and can lead to a depletion of ATP and to mitochondrial dysfunction (Tiwari et al., 2002). In turn, energy supply for ATP-dependent defense systems such as heat shock proteins and AAA-type proteases is considerably compromised under stress conditions. Our data suggest that organellar-targeted AARE provides an ATP-independent defense system to prevent or attenuate protein aggregation. Based on localization prediction, 70% of our selected plant species possess one AARE isoform that localizes to either plastids or to mitochondria (Table S1). Whether dual targeting *via* ambiguous targeting also occurs in these species remains to be investigated. Further, we cannot state whether the remaining species do not contain organellar targeted AARE isoforms or whether this assumption is due to incomplete gene models. Regarding this, we want to emphasize that gene annotations containing the plastid transit peptide were not present in earlier genome annotations

of Physcomitrella and Arabidopsis (Lamesch et al., 2012; Zimmer et al., 2013) but were introduced with later versions (Cheng et al., 2017; Lang et al., 2018). Thus, it is possible that localization of AARE isoforms to plastids and mitochondria is a deeply conserved feature within the plant kingdom.

It is not yet clear how translation of both variants in Arabidopsis is regulated, but a recent study on Arabidopsis riboproteogenomics highlighted the importance of alternative translation initiation in shaping different subcellular localizations or functions of proteoforms (Willems et al., 2021). This mechanism is also present in Physcomitrella, where dual targeting of FtsZ isoforms to the cytoplasm and plastids is enabled *via* alternative translation initiation (Kiessling et al., 2004). Thus, localization of PpAARE1 to the cytoplasm is also possible from the longer splice variant. Alternative translation initiation of AtAARE is further evidenced by publicly available proteomics data (www.peptideatlas.org/builds/arabidopsis/, van Wijk et al., 2021). Here, we found peptide evidence for N-terminal acetylation of M^{56} which is the initiator methionine of the short variant (e.g., Zhang et al., 2019, PXD012708). In contrast, no peptide evidence was found covering the longer ORF. N^{α}-acetylation of plant proteins occurs either co-translationally on the N-terminus emerging from the ribosome or post-translationally after import into plastids and cleavage of the targeting peptide (Linster & Wirtz, 2018). Since the subsequent amino acid of the acetylated methionine (M^{56}) is aspartic acid (D), this would represent a target for the N-terminal acetyltransferase complex B (NatB). This complex is associated with cytosolic ribosomes and mediates co-translational acetylation of methionine residues followed by aspartic or glutamic acid (Polevoda et al., 2008). In this respect, the N^{α}-acetylation of M^{56} indicates an alternative translation initiation from this internal methionine of the shorter ORF.

Nakai et al. (2012) used the shorter open reading frame for localization analysis and observed the fluorescent reporter fusion of AtAARE in the cytoplasm and in the nucleus. The latter localization was not observed for AtAARE in our study. Consequently, the question is whether AtAARE cannot localize to the nuclei of Physcomitrella protoplasts or whether certain conditions are necessary. With a molecular weight of 111.1 kDa (AtAARE:eGFP, short ORF variant fused to eGFP) the fusion protein is beyond the limit for passive diffusion across the nuclear membrane (Macara, 2001). Using the predictor *LOCALIZER* (Sperschneider et al., 2017) we identified an NLS (Table S1) which would enable active transport into the nucleus. Accordingly, we also identified NLS in PpAARE1 and PpAARE3, but not in PpAARE2. Nevertheless, here we also did not observe nuclear localization of the fusion proteins. The human AARE homolog, HsACPH, does not have any predictable NLS, but nuclear import is mediated *via* interaction with XRCC1

under certain stress conditions (Zeng et al., 2017). Similarly, a nuclear localization of AARE isoforms might occur under certain stress conditions also *in planta*.

Among the three PpAARE isoforms, PpAARE1 is apparently the dominant isoform regarding exopeptidase activity (Fig. 5b, 7f), whereas PpAARE2 acts as endopeptidase. The operation mode of PpAARE3 is as yet unresolved, and it remains unanswered whether PpAARE2 exhibits exopeptidase activity. It is still not clear how the endopeptidase mode in AARE enzymes is implementable with the structural conformation due to the sterical hindrance of the beta-propeller. Crystal structures from bacterial and archaeal AARE isoforms revealed two possible entrances for substrates to the catalytic centers (Bartlam et al., 2004; Brocca et al., 2016) but the mode of substrate entry to the catalytic center is still not fully understood, especially of substrates like intact proteins. However, although the quaternary arrangements of subunits differ between species (Menyhárd et al., 2013; Brocca et al., 2016), the secondary structure arrangement seems conserved across kingdoms and specific subunit interactions (multimerization) are likely a common mechanism to mediate substrate specificity and to modulate activity. This could be further used as a switch between the endo- and exopeptidase mode and additionally enable accessibility of the catalytic center for larger molecules *via* structural re-arrangements. Accordingly, the interaction between the distinct PpAARE isoforms may represent a similar way to modify substrate specificity and/or activity. Here, we analyzed the interaction of the isoforms in protonema, but the data obtained in Hoernstein et al. (2016, Fig. S11d) was generated from gametophore cultures. Hence, we conclude that these interactions are not tissue-specific, but ubiquitous in Physcomitrella. Yet, the function of this interaction is unclear. It may be modulation of activity or substrate specificity or rather depend on differential expression and spatiotemporal coincidence. We exclude the possibility that interacting isoforms are targets for degradation of the respective bait isoform, since protease/target interactions are rather transient. However, it should be mentioned that proteolysis-based sub fragments of bovine lens AARE exist and exhibit catalytic activity on intact lens proteins (Senthilkumar et al., 2001).

Our data indicate a partial compensation between PpAARE1 and PpAARE2. Both single KO mutants appear phenotypically inconspicuous under normal conditions, although a significant reduction in the exopeptidase activity was observed in ΔPpAARE1 (Fig. 5). PpAARE2 seemed to have the strongest effect on the accumulation of oxidized proteins (Fig. 7g) in gametophores on the single isoform KO level, whereas the double KO showed the most striking effect in all lines. Intriguingly, this double KO results in a strongly affected gametophore growth and reduction of life span (Fig. 8). This phenotype partially resembles a loss-of-function mutant of a central

component of autophagy (PpATG3) in Physcomitrella (Chen et al., 2020). In ΔPpATG3, gametophores also exhibited a reduced life span and colonies were smaller than in WT. In contrast, gametophore size was not affected. Further, photosynthetic capacity in ΔPpATG3 was also reduced, an effect which is apparently not caused by AARE depletion (Nakai et al., 2012) and PpAARE genes were not differentially expressed in ΔPpATG3 (Chen et al., 2020). Thus, we conclude that the reduced life span observed in ΔPpAARE1/2 and ΔPpAARE1/3/2 is not due to an impaired autophagy system causing nitrogen starvation. This is in line with data, which opposes autophagy at the onset of senescence in Arabidopsis (Jia et al., 2019; Zentgraf, 2019).

In mammals, elevated levels of oxidized proteins are associated with several severe diseases, such as Alzheimer´s disease, different types of carcinomas and diabetes (Dalle-Donne et al., 2003). If proteolytic clearance fails, further accumulation of irreversible oxidized proteins causes protein aggregation, which is among the hallmarks of aging (López-Otín et al., 2013). Consequently, premature gametophore induction, reduced life span and increased levels of oxidized proteins, especially at the higher molecular weight range (Fig. 7g) in ΔPpAARE1/2 are signs of accelerated aging. The knockout of all three isoforms did not enhance these effects, indicating a minor effect of PpAARE3 under our conditions. Accelerated aging is further supported by the fact that in ΔPpAARE1/2 and ΔPpAARE1/3/2 the tip of the gametophores, which is younger tissue, is viable longer than the older stem (Fig. 8). As PpAARE3 cannot compensate the lack of PpAARE1 or PpAARE2, its functional significance remains unclear. This may pinpoint towards specific functions under stress conditions, requiring a detailed analysis of AARE action in stress responses. Abiotic stress such as heat, drought or strong light intensities are stimuli that increase ROS production, thereby causing enhanced protein oxidation. Although this could indicate an important role of AARE in stress responses, the expression of PpAARE genes is rather reduced or unaffected under heat in our data (Fig. S14) and in the data of Elzanati et al. (2020). In addition, a more detailed analysis during all stages of the life cycle may elucidate specific developmental regulations, as, for example, ROS are required for spore wall formation in Physcomitrella (Rabbi et al., 2020).

Protein oxidation related to aging is far less studied in plants than in mammals. Plastid ROS levels increase during aging (Munné-Bosch & Alegre, 2002), which is in line with strong oxidation of plastid proteins in aging leaves (Johannson et al., 2004). Likewise, protein oxidation marks the developmental transition between vegetative growth and flowering in Arabidopsis (Johannson et al., 2004). Here, we observed a different size distribution of oxidized proteins in Arabidopsis plants during vegetative growth (Fig. 12a) and in adult gametophores of Physcomitrella (Fig. 7g). This

difference may be due to species-specific differences, or to differences between gametophytic (moss) and sporophytic tissue (angiosperm). It is difficult to compare protein profiles from a whole-plant extract (here: Physcomitrella gametophores) with an extract from a selected part of a plant (here: Arabidopsis rosette leaves). An additional layer of complexity is likely introduced by the time of sampling or different metabolic states of the tissues. This is supported by conflicting findings, where studies describe the most prominent targets of oxidation either as plastid proteins (Johannson et al., 2004; Nakai et al., 2012) or as mitochondrial proteins (Bartoli et al., 2004). Nevertheless, the abolishment of AARE activity lead to increased levels of oxidized proteins and to a faster progression in the life cycle as a sign of aging in the moss and in the angiosperm.

Here, the AtAARE mutant exhibited increased levels of oxidized proteins under normal cultivation conditions and an accelerated developmental transition, in this case premature bolting (Fig. 12b). Intriguingly, we observed a premature induction of gametophore formation from protonema mainly in the double KOs of PpAARE1/2, which also exhibits a reduced lifespan and a strong accumulation of oxidized proteins. Age-related developmental transitions in plants such as meristem formation by time-resolved action of micro RNAs and hormonal crosstalk are well studied (Laufs et al., 2004; Wu & Poethig, 2006; Yant et al., 2010; Arif et al., 2012; Singh et al., 2014; reviewed in Rankenberg et al., 2021). Induction of bolting and flowering is tightly linked to temperature (Balasubramanian et al., 2006) and the transition from the vegetative to the reproductive phase is mediated *via* transcriptional regulation of FLOWERING LOCUS M (FLM) and SHORT VEGETATIVE PHASE (SVP, Lee et al., 2013; Posé et al., 2013). Central components of the transcriptional regulation of FLM are splicing factor 1 (AtSF1, Lee et al., 2020) and the U1 small nuclear ribonucleoprotein RBP45d (Chang et al., 2022). However, it is not yet fully resolved how temperature sensing is finally transmitted to cause this transcriptional regulation. Based on our data, we hypothesize that protein oxidation might represent a missing link between temperature sensing and regulation of developmental transitions in plants. In, turn AARE activity may reduce stress-related protein oxidation and thus delay aging and related developmental transitions from the vegetative to the generative phase in plants.

Material and Methods

Cultivation of Physcomitrella genotypes

Physcomitrella WT (new species name: *Physcomitrium patens* (Hedw.) Mitt.; Medina et al. (2019)), ecotype "Gransden 2004" and AARE KO lines were cultivated in Knop medium supplemented with microelements. Knop medium (pH 5.8) containing 250 mg/L KH_2PO_4, 250 mg/L KCl, 250 mg/L $MgSO_4$ x 7 H_2O, 1,000 mg/L $Ca(NO_3)_2$ x 4 H_2O and 12.5 mg/L $FeSO_4$ x 7 H_2O was prepared as described in Reski and Abel (1985) and supplemented with 10 mL per liter of a microelement (ME) stock solution (309 mg/L H_3BO_3, 845 mg/L $MnSO_4$ x 1 H_2O, 431 mg/L $ZnSO_4$ x 7 H_2O, 41.5 mg/L KI, 12.1 mg/L Na_2MoO_4 x 2 H_2O, 1.25 mg/L $CoSO_4$ x 5 H_2O, 1.46 mg/L $Co(NO_3)_2$ x 6 H_2O) as described by Egener et al. (2002) and Schween et al. (2003a). For cultivation on solid medium, 12 g/L Agar was added to the KnopME medium. Moss suspension cultures were disrupted weekly with an ULTRA-TURRAX (IKA) at 18,000 rpm for 90 s. If not indicated otherwise, moss was grown under standard light conditions (55 µmol photons/m^{2}s) at 22°C in a 16h/8h light/dark cycle.

Hydroponic Physcomitrella gametophore cultures were as described in Erxleben et al. (2012) and Hoernstein et al. (2016). In brief, a thin layer of protonema from suspension was spotted on gauze mesh (PP, 250 m mesh, 215 m thread, Zitt Thoma GmbH, Freiburg, Germany) capped on a glass ring. The glass rings with protonema-covered mesh gauze were placed in Magenta®Vessels (Sigma-Aldrich, St. Louis, USA) and KnopME medium was added until the protonema-covered gauze mesh was moist. The medium was exchanged every 4 weeks. Gametophores were harvested after 12 weeks.

Generation of AARE knockout lines

Knockout constructs for each AARE gene were generated by amplifying genomic regions as homologous flanks. The PCR products were fused to a neomycin (AARE1), hygromycin (AARE2) and zeocin (AARE3) resistance cassettes, respectively, employing triple template PCR described in Tian et al. (2004) with primer sequences listed in Table S2 using the *Q5* polymerase (New England Biolabs, Ipswich, USA). The knockout constructs were released from their vector backbones with XhoI (PpAARE1), BglII (PpAARE2) and DraI (PpAARE3), respectively. Enzymes were purchased from Thermo Fisher Scientific. Digested plasmids were precipitated and sterilized prior to transfection using standard ethanol precipitation method (Sambrook & Russell, 2006). Transfection of Physcomitrella WT or KO (for consecutive knockouts) protoplasts was conducted as described (Hohe & Reski, 2002; Hohe et al., 2004). The WT strain as well as the identified

35

PpAARE KO lines are accessible via the International Moss Stock Center (IMSC, www.moss-stock-center.org). IMSC accession numbers for the mutant and WT are available in Table S5.

Screening of plants surviving antibiotics selection was done by PCR. KO mutant plants surviving the antibiotics selection were checked for the presence of a genomic region which should be removed upon homologous recombination-based integration of the knockout construct (Fig. 4). In case of the absence of this WT signal, plants were further checked for correct 5' and 3' integration of the respective knockout construct using primers listed in Table S2.

Generation of PpAARE-Citrine knock-in lines

Knock-in constructs to fuse the coding sequence of Citrine to the C-terminus of PpAARE isoforms via an 18 bp linker (Tian et al., 2004) at the endogenous genomic locus were cloned via Gibson assembly as described (Gibson et al., 2009). All necessary parts were amplified using primers listed in Table S2. Additionally, XhoI (PpAARE1), SalI (PpAARE2) and BamHI (PpAARE3) restriction sites were added to the 5' and the 3' ends of the respective knock-in construct. All parts were assembled into pJet1.2 vector backbone (Thermo Scientific) using the Gibson Assembly®Cloning Kit from New England Biolabs (Ipswich, Massachusetts, USA). Transfection of Physcomitrella WT protoplasts were conducted as described (Hohe & Reski, 2002; Hohe et al., 2004) by co-transfecting a plasmid containing a neomycin phosphotransferase resistance (nptII) cassette as transient selection marker (pBSNNNEV, Mueller et al., 2014). The linearized plasmid and the co-transfection vector were purified and sterilized *via* ethanol precipitation (Sambrook & Russell, 2006) prior to transfection.

The presence of Citrine was checked with primers listed in Table S2 and resulting positive lines were further checked for correct 5' and 3' integration by PCR using the Plant Phire Kit with primers listed in Table S2. All identified fusion lines are available via the International Moss Stock Center (IMSC, www.moss-stock-center.org). IMSC accessions are listed in Table S5.

Cloning of fusion constructs for subcellular localization

All constructs were generated using Gibson assembly and integrated into a PpAct5:Linker:eGFP-MAV4 vector backbone described in Özdemir et al. (2018). Integration of the different coding sequences was done in frame in front of the Linker:eGFP. All parts for the Gibson assembly (inserts and corresponding vector backbones) were amplified either with Phusion™ polymerase (Thermo Fisher Scientific) or with HiFi polymerase (PCR Biosystems Ltd) according to the manufacturer´s instructions. The primers were designed to have a 25 bp overlap to the

corresponding fragment to be fused with. All primers and combinations are listed in Table S3. In the case of the N-terminal difference of AtAARE (M^1-A^{55} of AT4G14570.1, gene model provided by TAIR (https://www.arabidopsis.org/)) the Actin5 promotor was replaced by the CaMV35S promotor (Amack & Antunes, 2020) previously tested in Physcomitrella (Horstmann et al., 2004).

Cloned plasmids were purified using the PureYield™ Plasmid Midiprep kit (Promega, Wisconsin, USA) according to the manufacturer´s instructions. The plasmids were purified and sterilized *via* ethanol precipitation (Sambrook & Russell, 2006).

Confocal microscopy

Confocal imaging was performed on transiently transfected live protoplasts using Leica TCS SP8 (Leica Microsystems, Wetzlar, Germany). Immediately before microscopy, MitoTracker™ Orange CMTMRos (ThermoFisher Scientific) was added to protoplast suspensions to a final concentration of 100 nM. For all imaging experiments, an HC PL APO CS2 63x/1.40 OIL objective was used with a zoom factor of 4. The pinhole was set to 35.4 µm. For excitation, a WLL laser (70%) was used. In a sequential acquisition setup, eGFP and chlorophyll were excited with the same laser beam (488 nm, 2%) and their signals were detected simultaneously, whereas MitoTracker™ was excited with a different laser beam (550 nm, 2%) and its signal was detected separately. The detection ranges were specified as 502 nm - 546 nm for eGFP, 662 nm - 732 nm for chlorophyll and 597 nm - 636 nm for MitoTracker™. The images were acquired as z-stacks with the number of optical sections varying with the protoplast size. The voxel sizes of the resulting z-stacks were 0.0903, 0.0903, 0.239 µm in the x-y-z order. For visual representation and analysis, single slices with the best signal-to-noise ratio were selected and extracted from each z-stack using FIJI software.

qPCR analysis

The copy number of the integrated KO constructs was determined using a qPCR-based method as described in Noy-Malka et al. (2014). Genomic DNA was extracted from 100 mg frozen protonema using the GeneJEt Plant Genomic DNA Purification Kit (Thermo Scientific, Waltham, USA). DNA concentrations were adjusted to 3 ng/µl for each sample and qPCR was performed with primers for the 5' and the 3' flanks as well as with primers for the corresponding selection cassette. Additionally, primers for the single copy gene CLF (Pp3c22_2940V3) were used as internal control. Reference lines were WT as well as in-house lines with known single integrations of the used selection cassettes. Primers are listed in Table S4. PCR reactions were done using

2x SensiFAST Mix (Bioline, London, UK) and analyzed in a Lightcycler 480 II (Roche, Basel, Schweiz).

cDNA preparation

RNA was extracted using the innuPREP Plant RNA Kit (Analytik Jena, Jena, Germany). The extracted RNA was treated with DNAse I (Thermo Scientific) and subsequently reverse transcribed into cDNA using Superscript III Reverse Transcriptase (Life Technologies, Carlsbad, USA).

Cultivation of Arabidopsis genotypes

Seeds were surface-sterilized for 4 min in 80% ethanol and subsequently for 1 min in 100% ethanol. Seeds were placed on plates containing ½ MS supplemented with 1% (D+) sucrose and 0.8% Agar. Alternatively, seeds were directly placed on sterilized soil. Seeds were incubated at 8°C for 2-4 days in the dark for stratification before placing them in growth chambers. Plants were further cultivated under short day conditions at 22°C and 70 µmol photons/m^{2}s in an 8h/16h light/dark cycle. For bolting assays, plants were placed in a phyto chamber at 22°C and 70 µmol photons/m^{2}s in a 16h/8h light/dark cycle (long day condition). Rosette leaves and days since sowing were counted upon appearance of the shoot in the middle of the rosette.

Screening of Arabidopsis AARE mutants

Arabidopsis thaliana lines with T-DNA insertions in the At4G14570 locus were identified from the public T-DNA Express database at the SIGnAL website (Salk Institute Genomic Analysis Laboratory). Lines GK-456A10, SALK_080653C, SALK_071125C, and SALK_205137C, were obtained from the Nottingham Arabidopsis Stock Center. Homozygous mutant alleles were verified by PCR using the following primers: forward LB GK 5´-ATATTGACCATCATACTCATTGC-3´ and reverse GK-456 5´-CTTCAAAGAAACACCAATCAG-3´for the GK-456A10 line, and forward LB-pROK 5´-GCGTGGACCGCTTGCTGCAACT-3´ and reverse Salk_53 5´-TCTTTAGCCGAATCAGTTCCAGA-3´for the SALK_080653C, SALK_071125C, and SALK_205137C lines. Identified homozygous mutant plants were back-crossed with Arabidopsis Col-0. The F2 generation was screened for homozygous mutant plants using the above listed primer-sets to identify the mutant allele or substituting the forward primers with forward WT-GK-456 5´-AAGATGCTTTGCAGTCTCTA-3´ and forward WT-Salk 5´-ACTGCCTTATGATCCATTGTCTC-3´, to identify the GK and SALK lines WT alleles, respectively (primers combinations are further listed in Table S6. RT-PCR was additionally performed to check

38

for the presence of AtAARE transcripts using Taq polymerase on cDNA prepared as described above with primers At1-At4 (Table S6).

AARE exopeptidase activity in plant tissues

The enzyme activity assay of Yamauchi et al. (2003) was modified. In short, tissue was homogenized in liquid nitrogen and dissolved in 100 µL extraction buffer (50 mM PBS, 1 mM EDTA, 2 mM DTT) per 10 mg FW. After centrifugation at 20,000 x g for 20 min at 4°C, 5 µl supernatant was mixed with 195 µL reaction buffer (50 mM HEPES-KOH, pH 7.5 containing 1 mM Ac-Ala-pNA (Bachem, Bubendorf, Switzerland)) in a 96 well micro titer plate and incubated at 37°C for 30-120 min. In the case of Ac-Leu-pNA as substrate, 50 mM HEPES-KOH, pH 7.5 with 10% DMSO containing 1mM AcLeu-pNA (Bachem) was used as reaction buffer. Every sample was measured in three technical replicates. Absorbance was measured at 410 nm. Activity was calculated using a molar absorbance coefficient of 8.8 mM*cm^{-1} according to Nakai et al. (2012) and represents the release of pNA [µmol] per minute normalized to the total protein concentration of the sample. The protein concentration was determined using the A_{280} method of a NanoDrop^{TM} (Thermo Fisher Scientific) or with a Bradford assay (Bradford, 1976).

Western Blot

Western Blots were performed as described in Lang et al. (2011) using the *ECL Advance detection kit* (GE Healthcare). The primary antibody against *A. thaliana* AARE was kindly provided by Dr. Yasuo Yamauchi and is described in Yamauchi et al. (2003). The primary antibody was diluted 1:10,000 in TBST-Buffer with 2% Blocking (GE Healthcare) and incubated on the membrane for 2 h. As secondary antibody anti-Guinea pig antibody, coupled to a horseradish peroxidase (Agrisera, AS 10 1496) diluted 1:10,000 in 2% TBST with 2% Blocking (GE Healthcare), was applied for 1 h.

Detection of oxidized proteins

Plant tissues were homogenized in liquid nitrogen and proteins were extracted in 50 mM PBS, 50 mM DTT, 1mM EDTA. 3-6 µg total protein was derivatized with DNPH and subsequently detected with an anti-DNP antibody according to the manufacturer's instruction of the *OxyBlot Protein Oxidation Detectio*n Kit (S7150, Sigma-Aldrich). Equal amounts of the derivatized protein samples were employed as loading control on a separate SDS-gel and stained with Coomassie or silver staining.

Flow cytometry analysis

FCM analysis was performed according to Schween et al. (2003b). In brief, protonemata were chopped with a razor blade in a small petri dish (6 cm diameter) in 2 mL of DAPI-buffer containing 0.01 mg/L 4′,6-Diamidin-2-phenylindol (DAPI), 1.07 g/L $MgCl_2$ x 6 H_2O, 5 g/L NaCl, 21.11g/L Tris, 0.1% Triton, pH 7. The solution was filtered using 30 µm pore size filters and the fluorescence intensity was measured using a Cyflow®Space flow cytometry system (Partec, Munich, Germany).

Computational predictions

Predictions for the presence of cleavable targeting peptides were performed with *TargetP-2.0* (Armenteros et al., 2019). Additional predictions of subcellular localizations were performed with *LOCALIZER* (Sperschneider et al., 2017). The presence of peroxisomal targeting signals was predicted with *PredPlantPTS1* (Lingner et al., 2011; Reuman et al., 2012). Prediction of protein domains was performed using *InterProScan* (Blum et al., 2021) and protein domain annotations according to PFAM (Mistry et al., 2021) were used.

Co-Immunoprecipitation

Co-immunoprecipitation was performed using GFP-Trap Magnetic Particles M-270 (Chromotek, Planegg-Martinsried, Germany) as recommended by the manufacturer with modifications. 300 mg protonema was homogenized in a 2 mL reaction tube using a tungsten and a glass bead. For each line three biological replicates were realized. The extraction buffer was chosen according to the manufacturer's recommendations for plant samples and contained 25 mM HEPES-KOH, pH7.5, 2 mM EDTA, 100 mM NaCl, 200 nM DTT, 0.5% Triton X-100, 1% plant protease inhibitor cocktail (PPI, P9599, Sigma Aldrich). Ground plant material was dissolved in a final volume of 2 mL ice-cold extraction buffer and incubated for 10 min in a water quench ultrasonic device. Samples were centrifuged at 4°C at 20.00xg for 30 min. For each sample 25 µL magnetic particle slurry was washed with 500 µL extraction buffer. The sample supernatant was transferred to the cleaned beads and incubated, rotating for 1 h at 6°C. Subsequently, beads were washed with 1 mL extraction buffer without Triton and PPI and again with 500 µL. Beads were then dissolved in 500 µL wash buffer (10 mM Tris-HCl, pH7.5, 150 mM NaCl, 0.5 mM EDTA), transferred to a new reaction tube and washed again in 500 µL wash buffer. A RapiGest solution (0.2% in 50 mM Tris-HCl, pH7.5; RapiGest SF Surfactant (Waters, Milford, MA, USA) was mixed 3:1 with 5 mM DTT in 50 mM Tris-HCl, pH7.5. 30 µL of the resulting mixture were applied on each sample. Samples were incubated at 95°C for 5 min under continuous shaking. Samples were cooled down to RT and 5 µL of a trypsin (V5117, P) solution (0.025 µg/µL in 50 mM Tris-HCl, pH 7.5) were added to

each sample. Digestion on the beads was performed for 30 min at 32°C under continuous shaking. Supernatants were transferred to new reaction tubes and the remaining beads were washed twice with 50 µL 5 mM Iodoacetamide solution (in 50 mM Tris-HCl, pH7.5). The wash supernatants were combined with the trypsin-containing supernatant and incubated over night at 30°C under continuous shaking. Acid-catalyzed cleavage of the RapiGest surfactant was performed as recommended by the manufacturer. Samples were purified using C18-STAGE-Tips as described in Hoernstein et al. (2018) and eluted from the Tip in 30% ACN in 0.1% FA.

Mass spectrometry measurement and data analysis

MS analysis was performed on an Orbitrap Q-Exactive Plus instrument (Thermo Fisher Scientific) coupled to an UltiMate 3000 RSLCnano system (Dionex LC Packings/Thermo Fisher Scientific) as described in Top et al. (2021). Database search and label-free quantitation was performed using MaxQuant software V 1.6.0.16 (Cox & Mann, 2008) as described in Hoernstein et al. (2016). For each Co-IP a specific database was employed containing all V3.3 proteins of Physcomitrella (Lang et al., 2018) as well as the sequence of the fusion protein. Additionally, the contaminant list provided by the software was included. Decoys were generated on the fly by reverting the given protein sequences. Variable modifications were formation of pyro Glu (N term Q, −17.026549 Da), oxidation (M, +15.994915 Da), acetylation (N-term, +42.010565 Da) and deamidation (N, +0.9 84016 Da). Carbamidomethylation (C, +57. 021464 Da) was specified as fixed modification. Enzymatic specificity was set to tryptic with semi-specific free N-terminus. An FDR of 0.01 was set for protein identification. LFQ values (Cox et al., 2014) were used as quantitative values. Interaction analysis was performed in Perseus V 1.6.12.0 (Tyanova et al., 2016). Missing values were imputed from a normal distribution with a down-shift of 1.8 and distribution width of 0.3 (for histograms of imputed values see Fig. S12). Interaction partners were accepted at an FDR of 0.01 and a p-value less than 0.01.

The mass spectrometry proteomics data have been deposited at the ProteomeXchange Consortium via the PRIDE partner repository (Deutsch et al., 2020; Perez-Riverol et al., 2022) with the dataset identifier PXD033854.

Multiple sequence alignment and phylogenetic reconstruction

Homologous protein sequences were aligned with UPP (version 4.4.0; Nguyen et al., 2015) using default parameters and subsequently translated into a codon-aware CDS alignment with PAL2NAL (version 1.4; Suyama et al. 2006). Based on this multiple coding sequence alignment we reconstructed a maximum likelihood tree with RAxML (version 8.2.12; Stamatakis, 2014) using

the GTRCAT model with 1000 rapid bootstrap samples. The tree was rooted at the split between animal and plant sequences and plotted in R (R Core Team, 2022) using the packages ape (Paradis & Schliep, 2018) and ggtree (Yu et al., 2017).

Acknowledgements

Author contribution statement

S.N.W.H. designed research, performed experiments, analyzed data, and wrote the manuscript. B.Ö. and N.v.G. analyzed data and helped writing the manuscript. A.A.M. analyzed data. B.R.v.B., L.N., J.S.F., R.K., S.G., T.W., and F.S. performed experiments. M.R.F. and S.J.M.S. designed research and helped writing the manuscript. R.R. designed and supervised research, acquired funding, and wrote the manuscript. All authors approved the final version of the manuscript.

Declaration

The authors declare no competing interest.

References

Al-Khatib K, Paulsen GM (1989) Enhancement of thermal injury to photosynthesis in wheat plants and thylakoids by high light intensity. *Plant Physiology* 90: 1041-1048

Altschul SF, Madden TL, Schäffer AA, Zhang J, Zhang Z, Miller W, Lipman DJ (1997) Gapped BLAST and PSI-BLAST: a new generation of protein database search programs. *Nucleic Acids Research* 25: 3389-3402

Amack SC, Antunes MS (2020) CaMV35S promoter–a plant biology and biotechnology workhorse in the era of synthetic biology. *Current Plant Biology* 24: 100179

Arif MA, Fattash I, Ma ZR, Cho SH, Beike AK, Reski R, Axtell MJ, Frank W (2012) DICER-LIKE3 activity in *Physcomitrella patens* DICER-LIKE4 mutants cause severe developmental dysfunction and sterility. *Molecular Plant* 6: 1281-1294

Armenteros JJA, Salvatore M, Emanuelsson O, Winther O, von Heijne G, Elofsson A, Nielsen H (2019) Detecting sequence signals in targeting peptides using deep learning. *Life Science Alliance* 2: e201900429

Balasubramanian S, Sureshkumar S, Lempe J, Weigel D (2006) Potent induction of *Arabidopsis thaliana* flowering by elevated growth temperature. *PLOS GENETICS* 2: e106

Banks JA, Nishiyama T, Hasebe M, Bowman JL, Gribskov M, DePamphilis C, et al. (2011) The *Selaginella* genome identifies genetic changes associated with the evolution of vascular plants. *Science* 332: 960-963

Bartlam M, Wang G, Yang H, Gao R, Zhao X, Xie G, et al. (2004) Crystal structure of an acylpeptide hydrolase/esterase from *Aeropyrum pernix K1*. *Structure* 12: 1481-1488

Bartoli CG, Gómez F, Martinez DE, Guiamet JJ (2004) Mitochondria are the main target for oxidative damage in leaves of wheat (*Triticum aestivum* L.). *Journal of Experimental Botany* 55: 1663-1669

Bergamo P, Cocca E, Palumbo R, Gogliettino M, Rossi M, Palmieri G (2013) RedOx status, proteasome and APEH: Insights into anticancer mechanisms of t10, c12-conjugated linoleic acid isomer on A375 melanoma cells. *PLOS ONE* 8: e80900

Biswas MS, Mano JI (2015) Lipid peroxide-derived short-chain carbonyls mediate hydrogen peroxide-induced and salt-induced programmed cell death in plants. *Plant Physiology* 168: 885-898

Biswas MS, Fukaki H, Mori IC, Nakahara K, Mano JI (2019) Reactive oxygen species and reactive carbonyl species constitute a feed-forward loop in auxin signaling for lateral root formation. *Plant Journal* 100: 536-548

Blum M, Chang HY, Chuguransky S, Grego T, Kandasaamy S, Mitchell A, et al. (2021) The InterPro protein families and domains database: 20 years on. *Nucleic Acids Research* 49: D344-D354

Bowman JL, Kohchi T, Yamato KT, Jenkins J, Shu S, Ishizaki K, et al. (2017) Insights into land plant evolution garnered from the *Marchantia polymorpha* genome. *Cell* 171: 287-304

Bradford MM (1976) A rapid and sensitive method for the quantitation of microgram quantities of protein utilizing the principle of protein-dye binding. *Analytical Biochemistry* 72: 248-254

Brocca S, Ferrari C, Barbiroli A, Pesce A, Lotti M, Nardini M. (2016) A bacterial acyl aminoacyl peptidase couples flexibility and stability as a result of cold adaptation. *FEBS Journal* 283: 4310-4324

Brunialti EA, Gatti-Lafranconi P, Lotti M (2011) Promiscuity, stability and cold adaptation of a newly isolated acylaminoacyl peptidase. *Biochimie* 93: 1543-1554

Chang P, Hsieh HY, Tu SL (2022) The U1 snRNP component RBP45d regulates temperature-responsive flowering in Arabidopsis. *Plant Cell* 34: 834-851

Chen F, Mackey AJ, Stoeckert Jr CJ, Roos DS (2006) OrthoMCL-DB: querying a comprehensive multi-species collection of ortholog groups. *Nucleic Acids Research* 34: D363-D368

Chen Z, Wang W, Pu X, Dong X, Gao B, Li P, et al. (2020) Comprehensive analysis of the Ppatg3 mutant reveals that autophagy plays important roles in gametophore senescence in *Physcomitrella patens*. *BMC Plant Biology* 20: 440

Cheng CY, Krishnakumar V, Chan AP, Thibaud-Nissen F, Schobel S, Town CD (2017) Araport11: a complete reannotation of the *Arabidopsis thaliana* reference genome. *Plant Journal* 89: 789-804

Ciacka K, Tymiński M, Gniazdowska A, Krasuska U (2020) Carbonylation of proteins—an element of plant ageing. *Planta* 252: 12

Cox J, Mann M (2008) MaxQuant enables high peptide identification rates, individualized ppb-range mass accuracies and proteome-wide protein quantification. *Nature Biotechnology* 26: 1367-1372

Cox J, Hein MY, Luber CA, Paron I, Nagaraj N, Mann M (2014) Accurate proteome-wide label-free quantification by delayed normalization and maximal peptide ratio extraction, termed MaxLFQ. *Molecular & Cellular Proteomics* 13: 2513-2526

Dalle-Donne I, Giustarini D, Colombo R, Rossi R, Milzani A (2003) Protein carbonylation in human diseases. *Trends in Molecular Medicine* 9: 169-176

Dalle-Donne I, Carini M, Orioli M, Vistoli G, Regazzoni L, Colombo G, et al. (2009) Protein carbonylation: 2, 4-dinitrophenylhydrazine reacts with both aldehydes/ketones and sulfenic acids. *Free Radical Biology and Medicine* 46: 1411-1419

Deutsch, EW, Bandeira, N, Sharma, V, Perez-Riverol, Y, Carver, JJ, Kundu, DJ, et al. (2020). The ProteomeXchange consortium in 2020: enabling 'big data'approaches in proteomics. *Nucleic Acids Research*, 48: D1145-D1152

Egener T, Granado J, Guitton MC, Hohe A, Holtorf H, Lucht JM, et al. (2002) High frequency of phenotypic deviations in *Physcomitrella patens* plants transformed with a gene-disruption library. *BMC Plant Biology* 2: 6

El-Brolosy MA, Stainier DY (2017) Genetic compensation: A phenomenon in search of mechanisms. *PLOS GENETICS* 13: e1006780

Elzanati O, Mouzeyar S, Roche J (2020) Dynamics of the transcriptome response to heat in the moss, *Physcomitrella patens. International Journal of Molecular Sciences* 21: 1512

Erxleben A, Gessler A, Vervliet-Scheebaum M, Reski R (2012) Metabolite profiling of the moss *Physcomitrella patens* reveals evolutionary conservation of osmoprotective substances. *Plant Cell Reports* 31: 427-436

Farooq MA, Niazi AK, Akhtar J, Farooq M, Souri Z, Karimi N, Rengel Z (2019) Acquiring control: The evolution of ROS-Induced oxidative stress and redox signaling pathways in plant stress responses. *Plant Physiology and Biochemistry* 141: 353-369

Fernandez-Pozo N, Haas FB, Meyberg R, Ullrich KK, Hiss M, Perroud PF, et al. (2020) PEATmoss (Physcomitrella Expression Atlas Tool): a unified gene expression atlas for the model plant *Physcomitrella patens*. *Plant Journal* 102: 165-177

Fesenko IA, Arapidi GP, Skripnikov AY, Alexeev DG, Kostryukova ES, Manolov AI, et al. (2015) Specific pools of endogenous peptides are present in gametophore, protonema, and protoplast cells of the moss *Physcomitrella patens*. *BMC Plant Biology* 15: 87

Fesenko I, Seredina A, Arapidi G, Ptushenko V, Urban A, Butenko I, et al. (2016) The *Physcomitrella patens* chloroplast proteome changes in response to protoplastation. *Frontiers in Plant Science* 7: 1661

Foyer CH, Noctor G (2003) Redox sensing and signalling associated with reactive oxygen in chloroplasts, peroxisomes and mitochondria. *Physiologia Plantarum* 119: 355-364

Fujino T, Kojima M, Beppu M, Kikugawa K, Yasuda H, Takahashi K (2000) Identification of the cleavage sites of oxidized protein that are susceptible to oxidized protein hydrolase (OPH) in the primary and tertiary structures of the protein. *Journal of Biochemistry* 127: 1087-1093

Fuss J, Liegmann O, Krause K, Rensing SA (2013) Green targeting predictor and ambiguous targeting predictor 2: the pitfalls of plant protein targeting prediction and of transient protein expression in heterologous systems. *New Phytologist* 200: 1022-1033

Gibson DG, Young L, Chuang RY, Venter JC, Hutchison CA, Smith HO (2009) Enzymatic assembly of DNA molecules up to several hundred kilobases. *Nature Methods* 6: 343–345

Giorgi C, Marchi S, Simoes IC, Ren Z, Morciano G, Perrone M, et al. (2018) Mitochondria and reactive oxygen species in aging and age-related diseases. *International Review of Cell and Molecular Biology* 340: 209-344

Gogliettino M, Balestrieri M, Cocca E, Mucerino S, Rossi M, Petrillo M, et al. (2012) Identification and characterisation of a novel acylpeptide hydrolase from *Sulfolobus solfataricus*: structural and functional insights. *PLOS ONE* 7: e37921

Gogliettino M, Riccio A, Balestrieri M, Cocca E, Facchiano A, D'Arco TM, et al. (2014) A novel class of bifunctional acylpeptide hydrolases–potential role in the antioxidant defense systems of the Antarctic fish *Trematomus bernacchii*. *FEBS Journal* 281: 401-415

Gogliettino M, Cocca E, Sandomenico A, Gratino L, Iaccarino E, Calvanese L, et al. (2021) Selective inhibition of acylpeptide hydrolase in SAOS-2 osteosarcoma cells: is this enzyme a viable anticancer target? *Molecular Biology Reports* 48: 1505-1519

Gould SJ, Keller G A, Hosken N, Wilkinson J, Subramani S (1989) A conserved tripeptide sorts proteins to peroxisomes. *Journal of Cell Biology* 108: 1657-1664

Gratão PL, Polle A, Lea PJ, Azevedo RA (2005) Making the life of heavy metal-stressed plants a little easier. *Functional Plant Biology* 32: 481-494

Harman D (1956) Aging: A theory based on free radical and radiation chemistry. *Journal of Gerontology* 11: 298–300

Harman D (1972) The biologic clock: the mitochondria? *Journal of the American Geriatrics Society* 20: 145-147

Hoernstein SNW, Mueller SJ, Fiedler K, Schuelke M, Vanselow JT, Schuessele C, et al. (2016) Identification of targets and interaction partners of arginyl-tRNA protein transferase in the moss *Physcomitrella patens*. *Molecular & Cellular Proteomics* 15: 1808-1822

Hoernstein SNW, Fode B, Wiedemann G, Lang D, Niederkrüger H, Berg B, et al. (2018) Host cell proteome of *Physcomitrella patens* harbors proteases and protease inhibitors under bioproduction conditions. *Journal of Proteome Research* 17: 3749-3760

Hohe A, Reski R (2002) Optimisation of a bioreactor culture of the moss *Physcomitrella patens* for mass production of protoplasts. *Plant Science* 163: 69-74

Hohe A, Egener T, Lucht JM, Holtorf H, Reinhard C, Schween G, Reski R (2004) An improved and highly standardised transformation procedure allows efficient production of single and multiple targeted gene-knockouts in a moss, *Physcomitrella patens*. *Current Genetics* 44: 339-347

Hori K, Maruyama F, Fujisawa T, Togashi T, Yamamoto N, Seo M, et al. (2014) *Klebsormidium flaccidum* genome reveals primary factors for plant terrestrial adaptation. *Nature Communications* 5: 3978

Horstmann V, Huether CM, Jost W, Reski R, Decker EL (2004) Quantitative promoter analysis in *Physcomitrella patens*: a set of plant vectors activating gene expression within three orders of magnitude. *BMC Biotechnology* 4: 13

Islam MM, Ye W, Matsushima D, Munemasa S, Okuma E, Nakamura Y, et al. (2016) Reactive carbonyl species mediate ABA signaling in guard cells. *Plant and Cell Physiology* 57: 2552-2563

Jia M, Liu X, Xue H, Shi L, Wang R, Chen Y, et al. (2019) Noncanonical ATG8-ABS3 interaction controls senescence in plants. *Nature Plants* 5: 212-224

Johansson E, Olsson O, Nyström T (2004) Progression and specificity of protein oxidation in the life cycle of *Arabidopsis thaliana*. *Journal of Biological Chemistry* 279: 22204-22208

Kiessling J, Martin A, Gremillon L, Rensing SA, Nick P, Sarnighausen E, et al. (2004) Dual targeting of plastid division protein FtsZ to chloroplasts and the cytoplasm. *EMBO Reports* 5: 889-894

Kirbis A, Waller M, Ricca M, Bont Z, Neubauer A, Goffinet B, Szövényi P (2020) Transcriptional landscapes of divergent sporophyte development in two mosses, *Physcomitrium* (Physcomitrella) *patens* and *Funaria hygrometrica*. *Frontiers in Plant Science* 11: 747

Kiss AL, Hornung B, Rádi K, Gengeliczki Z, Sztáray B, Juhász T, et al. (2007) The acylaminoacyl peptidase from *Aeropyrum pernix* K1 thought to be an exopeptidase displays endopeptidase activity. *Journal of Molecular Biology* 368: 509-520

Lamesch P, Berardini TZ, Li D, Swarbreck D, Wilks C, Sasidharan R, et al. (2012) The Arabidopsis Information Resource (TAIR): improved gene annotation and new tools. *Nucleic Acids Research* 40: D1202-D1210

Lang EGE, Mueller SJ, Hoernstein SNW, Porankiewicz-Asplund J, Vervliet-Scheebaum M, Reski R (2011) Simultaneous isolation of pure and intact chloroplasts and mitochondria from moss as the basis for sub-cellular proteomics. *Plant Cell Reports* 30: 205–215

Lang D, Ullrich KK, Murat F, Fuchs J, Jenkins J, Haas FB, et al. (2018) The *Physcomitrella patens* chromosome-scale assembly reveals moss genome structure and evolution. *Plant Journal* 93: 515-533

Laufs P, Peaucelle A, Morin H, Traas J (2004) MicroRNA regulation of the CUC genes is required for boundary size control in Arabidopsis meristems. *Development* 131: 4311-4322

Lee JH, Ryu HS, Chung KS, Posé D, Kim S, Schmid M, Ahn JH (2013) Regulation of temperature-responsive flowering by MADS-box transcription factor repressors. *Science* 342: 628-632

Lee KC, Chung KS, Lee HT, Park JH, Lee JH, Kim JK (2020) Role of Arabidopsis splicing factor SF1 in temperature-responsive alternative splicing of FLM pre-mRNA. *Frontiers in Plant Science* 11: 1917

Levey S, Wingler A (2005) Natural variation in the regulation of leaf senescence and relation to other traits in Arabidopsis. *Plant, Cell & Environment* 28: 223-231

Lingner T, Kataya AR, Antonicelli GE, Benichou A, Nilssen K, Chen XY, et al. (2011) Identification of novel plant peroxisomal targeting signals by a combination of machine learning methods and *in vivo* subcellular targeting analyses. *Plant Cell* 23: 1556-1572

Linster E, Wirtz M (2018) N-terminal acetylation: an essential protein modification emerges as an important regulator of stress responses. *Journal of Experimental Botany* 69: 4555-4568

López-Otín C, Blasco MA, Partridge L, Serrano M, Kroemer G (2013) The hallmarks of aging. *Cell* 153: 1194-1217

Lorenz S, Tintelnot S, Reski R, Decker EL (2003) Cyclin D-knockout uncouples developmental progression from sugar availability. *Plant Molecular Biology* 53: 227-236

Macara IG (2001) Transport into and out of the nucleus. *Microbiology and Molecular Biology Reviews* 65: 570-594

Mao C, Zhu Y, Cheng H, Yan H, Zhao L, Tang J, et al. (2018) Nitric oxide regulates seedling growth and mitochondrial responses in aged oat seeds. *International Journal of Molecular Sciences* 19: 1052

Marshall I, Prince D, Johnson H, Ruiz D, Nicholaou M, Covey TM (2019) Analyzing the activity and expression of acyl peptide enzyme hydrolase (APEH) in the blood serum of patients with type II diabetes. *Bios* 90: 70-78

Maxwell DP, Wang Y, McIntosh L (1999) The alternative oxidase lowers mitochondrial reactive oxygen production in plant cells. *Proceedings of the National Academy of Sciences U.S.A.* 96: 8271-8276

Medina R, Johnson MG, Liu Y, Wickett NJ, Shaw J, Goffinet B (2019) Phylogenomic delineation of *Physcomitrium* (Bryophyta: Funariaceae) based on targeted sequencing of nuclear exons and their flanking regions rejects the retention of *Physcomitrella*, *Physcomitridium* and *Aphanorrhegma*. *Journal of Systematics and Evolution* 57: 404-417

Merchant SS, Prochnik SE, Vallon O, Harris EH, Karpowicz SJ, Witman GB, et al. (2007) The *Chlamydomonas* genome reveals the evolution of key animal and plant functions. *Science* 318: 245-250

Mergner J, Frejno M, List M, Papacek M, Chen X, Chaudhary A, et al. (2020) Mass-spectrometry-based draft of the *Arabidopsis* proteome. *Nature* 579: 409-414

Menyhárd DK, Kiss-Szemán A, Tichy-Rács É, Hornung B, Rádi K, Szeltner Z, et al. (2013) A self-compartmentalizing hexamer serine protease from *Pyrococcus horikoshii*: substrate selection achieved through multimerization. *Journal of Biological Chemistry* 288: 17884-17894

Mistry J, Chuguransky S, Williams L, Qureshi M, Salazar GA, Sonnhammer EL, et al. (2021) Pfam: The protein families database in 2021. *Nucleic Acids Research* 49: D412-D419

Mogk A, Tomoyasu T, Goloubinoff P, Rüdiger S, Röder D, Langen H, Bukau B (1999) Identification of thermolabile *Escherichia coli* proteins: prevention and reversion of aggregation by DnaK and ClpB. *EMBO Journal* 18: 6934-6949

Mogk A, Bukau B, Kampinga HH (2018) Cellular handling of protein aggregates by disaggregation machines. *Molecular Cell* 69: 214-226

Møller IM (2001) Plant mitochondria and oxidative stress: electron transport, NADPH turnover, and metabolism of reactive oxygen species. *Annual Review of Plant Biology* 52: 561-591

Møller IM, Jensen PE, Hansson A (2007) Oxidative modifications to cellular components in plants. *Annual Review of Plant Biology* 58: 459-481

Mueller SJ, Lang D, Hoernstein SNW, Lang EGE, Schuessele C, Schmidt A, et al. (2014) Quantitative analysis of the mitochondrial and plastid proteomes of the moss *Physcomitrella patens* reveals protein macrocompartmentation and microcompartmentation. *Plant Physiology* 164: 2081-2095

Müller-Schüssele SJ, Wang R, Gütle DD, Romer J, Rodriguez-Franco M, Scholz M, et al. (2020) Chloroplasts require glutathione reductase to balance reactive oxygen species and maintain efficient photosynthesis. *Plant Journal* 103: 1140-1154

Munné-Bosch S, Alegre L (2002) Plant aging increases oxidative stress in chloroplasts. *Planta* 214: 608-615

Nakai A, Yamauchi Y, Sumi S, Tanaka K. (2012) Role of acylamino acid-releasing enzyme/oxidized protein hydrolase in sustaining homeostasis of the cytoplasmic antioxidative system. *Planta* 236: 427–436

Nguyen ND, Mirarab S, Kumar K, Warnor T (2015) Ultra-large alignments using phylogeny-aware profiles. *Genome Biology* 16: 124

Noctor G, Veljovic-Jovanovic S, Driscoll S, Novitskaya L, Foyer CH (2002) Drought and oxidative load in the leaves of C3 plants: a predominant role for photorespiration? *Annals of Botany* 89: 841-850

Noy-Malka C, Yaari R, Itzhaki R, Mosquna A, Gershovitz NA, Katz A, Ohad N (2014) A single CMT methyltransferase homolog is involved in CHG DNA methylation and development of *Physcomitrella patens*. *Plant Molecular Biology* 84: 719-735

Orr MW, Mao Y, Storz G, Qian SB (2020) Alternative ORFs and small ORFs: shedding light on the dark proteome. *Nucleic Acids Research* 48: 1029-1042

Ostendorf AK, van Gessel N, Malkowsky Y, Sabovljevic MS, Rensing SA, Roth-Nebelsick A, Reski R (2021) Polyploidization within the Funariaceae – a key principle behind speciation, sporophyte reduction and the high variance of spore diameters? *Bryophyte Diversity and Evolution* 43: 164-179

Ouyang S, Zhu W, Hamilton J, Lin H, Campbell M, Childs K, et al. (2007) The TIGR rice genome annotation resource: improvements and new features. *Nucleic Acids Research* 35: D883-D887

Özdemir B, Asgharzadeh P, Birkhold AI, Mueller SJ, Röhrle O, Reski R (2018) Cytological analysis and structural quantification of FtsZ1-2 and FtsZ2-1 network characteristics in *Physcomitrella patens*. *Scientific Reports* 8: 11165

Palmieri G, Bergamo P, Luini A, Ruvo M, Gogliettino M, Langella E, et al. (2011) Acylpeptide hydrolase inhibition as targeted strategy to induce proteasomal down-regulation. *PLOS ONE* 6: e25888

Palmieri G, Cocca E, Gogliettino M, Valentino R, Ruvo M, Cristofano G, et al. (2017) Low erythrocyte levels of proteasome and acyl-peptide hydrolase (APEH) activities in Alzheimer's disease: a sign of defective proteostasis? *Journal of Alzheimer's Disease* 60: 1097-1106

Palumbo R, Gogliettino M, Cocca E, Iannitti R, Sandomenico A, Ruvo M, et al. (2016) APEH inhibition affects osteosarcoma cell viability via downregulation of the proteasome. *International Journal of Molecular Sciences* 17: 1614

Paradis E, Schliep K (2018) ape 5.0: an environment for modern phylogenetics and evolutionary analyses in R. *Bioinformatics* 35: 526-528

Parsell DA, Kowal AS, Singer MA, Lindquist S (1994) Protein disaggregation mediated by heat-shock protein Hspl04. *Nature* 372: 475-478

Perez-Riverol, Y, Bai, J, Bandla, C, García-Seisdedos, D, Hewapathirana, S, Kamatchinathan, S, et al. (2022). The PRIDE database resources in 2022: a hub for mass spectrometry-based proteomics evidences. *Nucleic Acids Research*, 50: D543-D552

Perroud PF, Haas FB, Hiss M, Ullrich KK, Alboresi A, Amirebrahimi M, et al. (2018) The *Physcomitrella patens* gene atlas project: large-scale RNA-seq based expression data. *Plant Journal* 95: 168-182

Petriv, I, Tang, L, Titorenko, VI, Rachubinski, RA (2004). A new definition for the consensus sequence of the peroxisome targeting signal type 2. *Journal of Molecular Biology*, 341: 119-134

Polevoda B, Brown S, Cardillo TS, Rigby S, Sherman F (2008) Yeast Nα-terminal acetyltransferases are associated with ribosomes. *Journal of Cellular Biochemistry* 103: 492-508

Polgar L (2002) The prolyl oligopeptidase family. *Cellular and Molecular Life Sciences* 59: 349-362

Posé D, Verhage L, Ott F, Yant L, Mathieu J, Angenent GC, et al. (2013) Temperature-dependent regulation of flowering by antagonistic FLM variants. *Nature* 503: 414-417

Queitsch C, Hong SW, Vierling E, Lindquist S (2000) Heat shock protein 101 plays a crucial role in thermotolerance in Arabidopsis. *Plant Cell* 12: 479-492

R Core Team (2022) R: A language and environment for statistical computing. R Foundation for Statistical Computing, Vienna, Austria. URL https://www.R-project.org/.

Rabbi F, Renzaglia KS, Ashton NW, Suh DY (2020) Reactive oxygen species are required for spore wall formation in *Physcomitrella patens*. *Botany* 98: 575–587

Rankenberg T, Geldhof B, van Veen H, Holsteens K, van de Poel B, Sasidharan R (2021) Age-dependent abiotic stress resilience in plants. *Trends in Plant Science* 26: 692-705

Ratajczak E, Małecka A, Ciereszko I, Staszak AM (2019) Mitochondria are important determinants of the aging of seeds. *International Journal of Molecular Sciences* 20: 1568

Rawlings ND, Polgar L, Barrett AJ (1991) A new family of serine-type peptidases related to prolyl oligopeptidase. *Biochemical Journal* 279: 907-908

Rawlings ND, Barrett AJ, Thomas PD, Huang X, Bateman A, Finn RD (2018) The MEROPS database of proteolytic enzymes, their substrates and inhibitors in 2017 and a comparison with peptidases in the PANTHER database. *Nucleic Acids Research* 46: D624-D632

Reski R, Abel WO (1985) Induction of budding on chloronemata and caulonemata of the moss, *Physcomitrella patens*, using isopentenyladenine. *Planta* 165: 354-358

Reumann, S (2004) Specification of the peroxisome targeting signals type 1 and type 2 of plant peroxisomes by bioinformatics analyses. *Plant Physiology* 135: 783-800

Reumann S, Buchwald D, Lingner T (2012) PredPlantPTS1: a web server for the prediction of plant peroxisomal proteins. *Frontiers in Plant Science* 3: 194

Riccio A, Gogliettino M, Palmieri G, Balestrieri M, Facchiano A, Rossi M, et al. (2015) A new APEH cluster with antioxidant functions in the antarctic hemoglobinless icefish *Chionodraco hamatus. PLOS ONE* 10: e0125594

Sambrook J, Russell DW (2006) Standard ethanol precipitation of DNA in microcentrifuge tubes. *Cold Spring Harbor Protocols* 2006: pdb-prot4456

Scaloni A, Jones W, Pospischil M, Sassa S, Schneewind O, Popowicz AM, et al. (1992) Deficiency of acylpeptide hydrolase in small-cell lung carcinoma cell lines. *Journal of Laboratory and Clinical Medicine* 120: 546-552

Schuessele C, Hoernstein SNW, Mueller SJ, Rodriguez-Franco M, Lorenz T, Lang D, Igloi G, Reski R (2016) Spatio-temporal patterning of arginyl-tRNA protein transferase (ATE) contributes to gametophytic development in a moss. *New Phytologist* 209: 1014–1027

Schween G, Hohe A, Koprivova A, Reski R (2003a) Effects of nutrients, cell density and culture techniques on protoplast regeneration and early protonema development in a moss, *Physcomitrella patens. Journal of Plant Physiology* 160: 209–212

Schween G, Gorr G, Hohe A, Reski R (2003b) Unique tissue-specific cell cycle in *Physcomitrella. Plant Biology* 5: 50–58

Sharma P, Jha AB, Dubey RS, Pessarakli M (2012) Reactive oxygen species, oxidative damage, and antioxidative defense mechanism in plants under stressful conditions. *Journal of Botany* 2012: 217037

Senthilkumar R, Reddy PN, Sharma KK (2001) Studies on trypsin-modified bovine and human lens acylpeptide hydrolase. *Experimental Eye Research* 72: 301-310

Santhoshkumar P, Kannan R, Sharma KK (2015) Proteases in lens and cataract. In: Studies on the Cornea and Lens (pp. 221-238). Humana Press, New York, NY.

Shimizu K, Fujino T, Ando K, Hayakawa M, Yasuda H, Kikugawa K (2003) Overexpression of oxidized protein hydrolase protects COS-7 cells from oxidative stress-induced inhibition of cell growth and survival. *Biochemical and Biophysical Research Communications* 304: 766-771

Singh A, Singh S, Panigrahi KCS, Reski R, Sarkar AK (2014) Balanced activity of microRNA166/165 and its target transcripts from the class III homeodomain-leucine zipper family regulates root growth in *Arabidopsis thaliana*. *Plant Cell Reports* 33: 945-953

Smakowska E, Czarna M, Janska H (2014) Mitochondrial ATP-dependent proteases in protection against accumulation of carbonylated proteins. *Mitochondrion* 19: 245-251

Smirnoff N (2000) Ascorbic acid: metabolism and functions of a multi-facetted molecule. *Current Opinion in Plant Biology* 3: 229-235

Soares C, Carvalho ME, Azevedo RA, Fidalgo F (2019) Plants facing oxidative challenges—A little help from the antioxidant networks. *Environmental and Experimental Botany* 161: 4-25

Sperschneider J, Catanzariti AM, DeBoer K, Petre B, Gardiner DM, Singh KB, et al. (2017) LOCALIZER: subcellular localization prediction of both plant and effector proteins in the plant cell. *Scientific Reports* 7: 44598

Stamatakis A (2014) RAxML version 8: a tool for phylogenetic analysis and post-analysis of large phylogenies. *Bioinformatics* 30: 1312–1313

Suyama M, Torrents D, Bork P (2006) PAL2NAL: robust conversion of protein sequence alignments into the corresponding codon alignments. *Nucleic Acids Research* 34: W609–W612

Sweetlove LJ, Heazlewood JL, Herald V, Holtzapffel R, Day DA, Leaver CJ, Millar AH (2002) The impact of oxidative stress on Arabidopsis mitochondria. *Plant Journal* 32: 891-904

Szeltner Z, Kiss AL, Domokos K, Harmat V, Náray-Szabó G, Polgár L (2009) Characterization of a novel acylaminoacyl peptidase with hexameric structure and endopeptidase activity. *Biochimica et Biophysica Acta (BBA)-Proteins and Proteomics* 1794: 1204-1210

Tangri A, Lighty K, Loganathan J, Mesmar F, Podicheti R, Zhang C, et al. (2021) Deubiquitinase UCHL1 maintains protein homeostasis through the PSMA7–APEH–Proteasome axis in high-grade serous ovarian carcinoma. *Molecular Cancer Research* 19: 1168-1181

Tian GW, Mohanty A, Chary SN, Li S, Paap B, Drakakaki G, et al. (2004) High-throughput fluorescent tagging of full-length *Arabidopsis* gene products in planta. *Plant Physiology* 135: 25-38

Tiwari BS, Belenghi B, Levine A (2002) Oxidative stress increased respiration and generation of reactive oxygen species, resulting in ATP depletion, opening of mitochondrial permeability transition, and programmed cell death. *Plant Physiology* 128: 1271-1281

Tola AJ, Jaballi A, Missihoun TD (2021) Protein carbonylation: Emerging roles in plant redox biology and future prospects. *Plants* 10: 1451

Top O, Milferstaedt SW, van Gessel N, Hoernstein SNW, Özdemir B, Decker EL, Reski R (2021) Expression of a human cDNA in moss results in spliced mRNAs and fragmentary protein isoforms. *Communications Biology* 4: 964

Tsunasawa S, Narita K, Ogata K (1975) Purification and properties of acylamino acid-releasing enzyme from rat liver. *Journal of Biochemistry* 77: 89-102

Tuskan GA, DiFazio S, Jansson S, Bohlmann J, Grigoriev I, Hellsten U, et al. (2006) The genome of black cottonwood, *Populus trichocarpa* (Torr. & Gray). *Science* 313: 1596-1604

Tyanova S, Temu T, Sinitcyn P, Carlson A, Hein MY, Geiger T, et al. (2016) The Perseus computational platform for comprehensive analysis of (prote)omics data. *Nature Methods* 13: 731-740

van Wijk KJ, Leppert T, Sun Q, Boguraev SS, Sun Z, Mendoza L, Deutsch EW (2021) The Arabidopsis PeptideAtlas: Harnessing worldwide proteomics data to create a comprehensive community proteomics resource. *Plant Cell* 33: 3421-3453

Varshavsky A (2011) The N-end rule pathway and regulation by proteolysis. *Protein Science* 20: 1298-1345

Varshavsky A (2019) N-degron and C-degron pathways of protein degradation. *Proceedings of the National Academy of Sciences U.S.A.* 116: 358-366

Wang J, Wang Y, Gao C, Jiang L, Guo D (2017) PPero, a computational model for plant PTS1 type peroxisomal protein prediction. *PLOS ONE* 12: e0168912

Wang QL, Chen JH, He NY, Guo FQ (2018) Metabolic reprogramming in chloroplasts under heat stress in plants. *International Journal of Molecular Sciences* 19: 849

Waszczak C, Carmody M, Kangasjärvi J (2018). Reactive oxygen species in plant signaling. *Annual Review of Plant Biology* 69: 209-236

Weise A, Rodriguez-Franco M, Timm B, Hermann M, Link S, Jost W, Gorr G (2006) Use of *Physcomitrella patens* actin 5′ regions for high transgene expression: importance of 5′ introns. *Applied Microbiology and Biotechnology* 70: 337-345

Willems P, Ndah E, Jonckheere V, van Breusegem F, van Damme P (2021) To new beginnings: Riboproteogenomics discovery of N-terminal proteoforms in *Arabidopsis thaliana*. *Frontiers in Plant Science* 12: 778804

Wu G, Poethig RS (2006) Temporal regulation of shoot development in *Arabidopsis thaliana* by miR156 and its target SPL3. *Development* 131: 3539–3547

Yamauchi Y, Ejiri Y, Toyoda Y, Tanaka K (2003) Identification and biochemical characterization of plant acylamino acid–releasing enzyme. *Journal of Biochemistry* 134: 251-257

Yamin R, Zhao C, O'Connor PB, McKee AC, Abraham CR (2009) Acyl peptide hydrolase degrades monomeric and oligomeric amyloid-beta peptide. *Molecular Neurodegeneration* 4: 33

Yant L, Mathieu J, Dinh TT, Ott F, Lanz C, Wollmann H, et al. (2010) Orchestration of the floral transition and floral development in Arabidopsis by the bifunctional transcription factor APETALA2. *Plant Cell* 22: 2156-2170

Yu G, Smith D, Zhu H, Guan Y, Lam TT (2017) ggtree: an R package for visualization and annotation of phylogenetic trees with their covariates and other associated data. *Methods in Ecology and Evolution* 8: 28-36

Zeng Z, Rulten SL, Breslin C, Zlatanou A, Coulthard V, Caldecott KW (2017) Acylpeptide hydrolase is a component of the cellular response to DNA damage. *DNA Repair* 58: 52-61

Zentgraf U (2019) Tug-of-war during senescence. *Nature Plants* 5: 129-130

Zhang H, Liu P, Guo T, Zhao H, Bensaddek D, Aebersold R, Xiong L (2019) Arabidopsis proteome and the mass spectral assay library. *Scientific Data* 6: 278

Zimmer AD, Lang D, Buchta K, Rombauts S, Nishiyama T, Hasebe M, et al. (2013) Reannotation and extended community resources for the genome of the non-seed plant *Physcomitrella patens* provide insights into the evolution of plant gene structures and functions. *BMC Genomics* 14: 498

Zybailov B, Rutschow H, Friso G, Rudella A, Emanuelsson O, Sun Q, van Wijk KJ (2008) Sorting signals, N-terminal modifications, and abundance of the chloroplast proteome. *PLOS ONE* 3: e1994

Supplemental figures
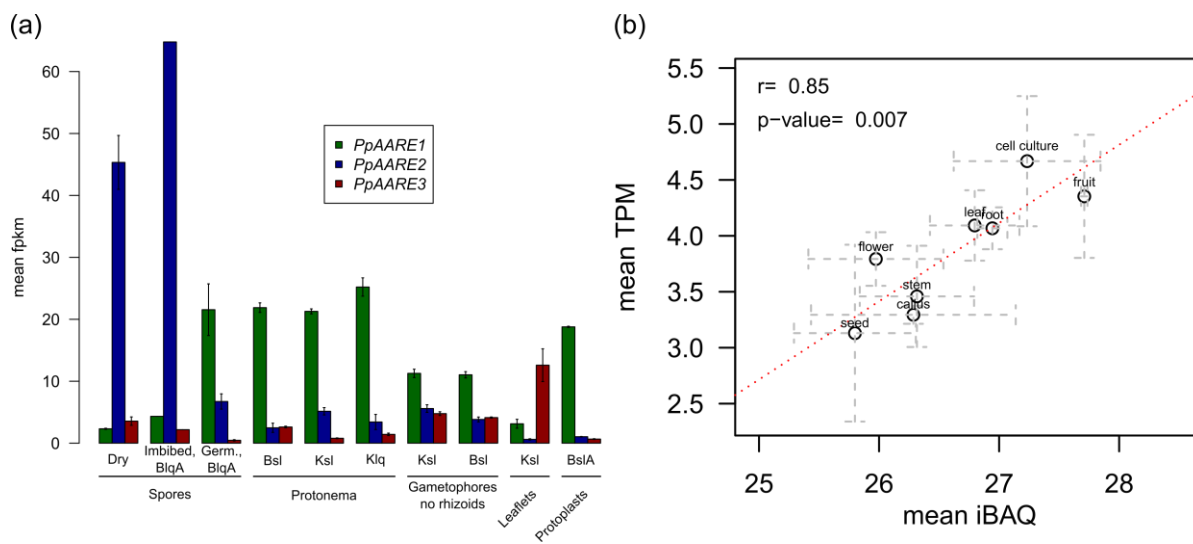
Figure S1 Tissue-specific expression levels of PpAARE genes and AtAARE. (a) Expression levels of the three PpAARE isoforms in different tissue and cell culture types. Depicted are mean FPKM values with standard error (Perroud et al., 2018; Fernandez-Pozo et al., 2020). All data has been downloaded from *PEATmoss* (https://peatmoss.online.uni-marburg.de/). Abbreviations: B = BCD medium (Ashton et al., 1979); lq = liquid; A =ammonium tartrate; sl = solid; K = Knop medium; Germ. = germinating. (b) Tissue-specific expression levels of AtAARE and correlation between protein abundance and transcript level in Columbia WT (Col0). Transcript and protein abundance data have been downloaded from the *ATHENA* database (http://athena.proteomics.wzw.tum.de/) and were generated by Mergner et al. (2020). Transcript levels are represented by transcripts per million kilobase (TPM) and protein abundances are represented as intensity based absolute quantification values (iBAQ). Data points are mean values with standard deviation for each tissue group as obtained from *ATHENA*. Pearson´s correlation (r = 0.85) indicates a strong positive and significant (p-value = 0.007) correlation of expression levels and protein abundance in major tissue types.
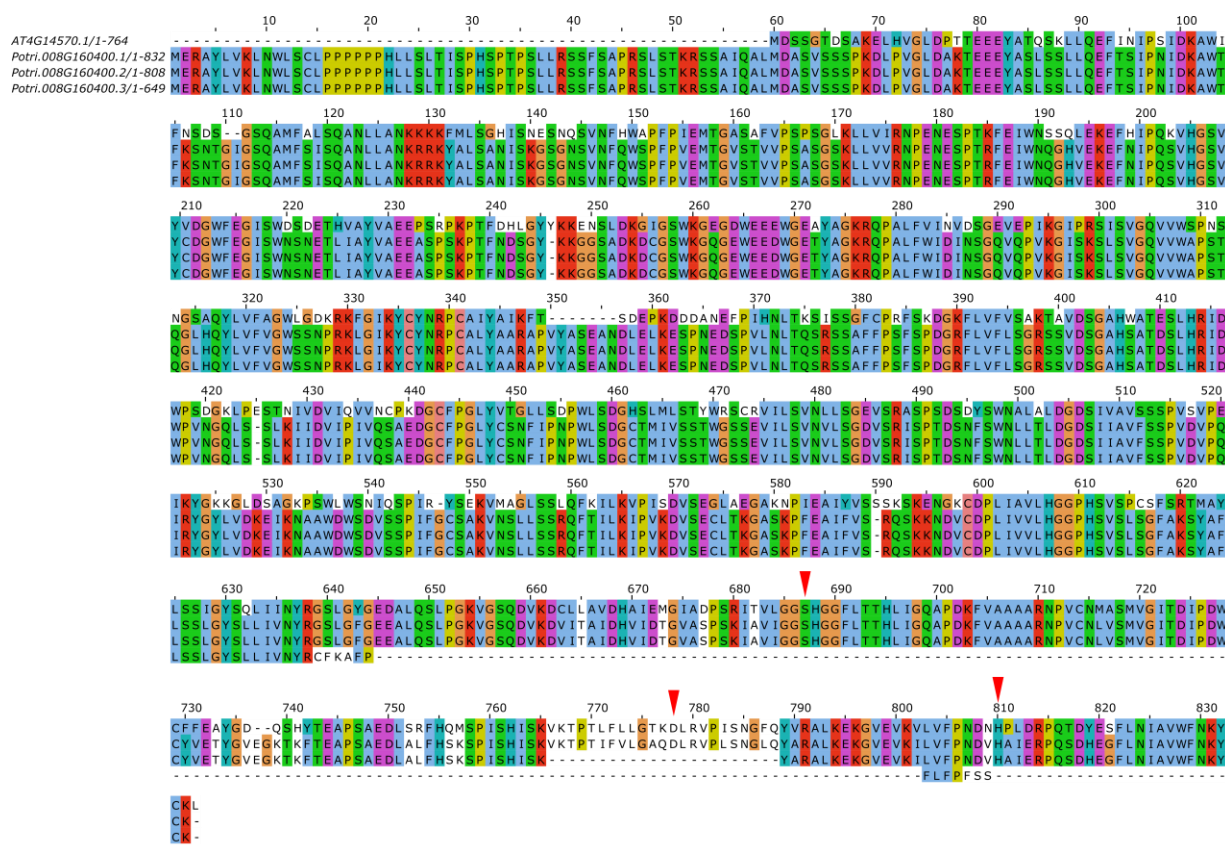
Figure S2 Sequence alignment of AtAARE and PtAARE isoforms. Red arrows point to the catalytic residues (Ser, Asp, His) of AtAARE as described in Yamauchi et al. (2003). Two splice variants result in nonfunctional protein isoforms. Potri.008G160400.2 lacks the catalytic Asp (alignment position 778) and Potri.008G160400.3 is lacking the whole catalytic domain. Sequences were aligned in Jalview (Version: 2.11.1.3, Waterhouse et al., 2009) using T-Coffee (Notredame et al., 2000) with default settings.
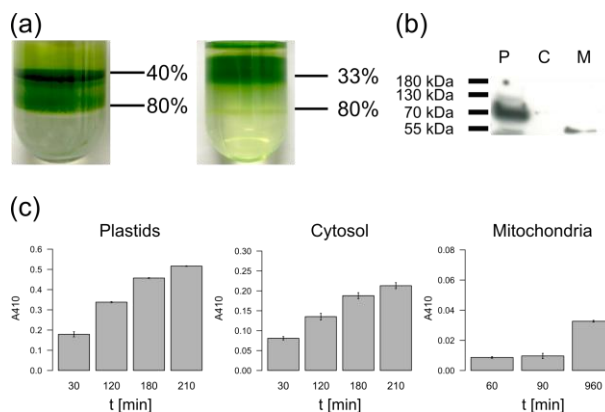
Figure S3 AARE activity in Physcomitrella plastids and mitochondria. (a) Plastids and mitochondria were simultaneously isolated from the protonema as described in Lang et al. (2011). Intact plastids were collected at the interface between 80% and 40% Percoll, mitochondria were collected at the interface between 80% and 33% Percoll. (b) Cross-contamination of the obtained fractions with plastid proteins was assessed via Western Blot against the plastid HSP70B (Agrisera, AS06 175). Fractions were soluble plastid proteins (P), the soluble fraction depleted of plastids and mitochondria (referred to as cytosol, (C)) and soluble mitochondrial proteins (M). The intracellular and mitochondrial fraction was free of plastid cross-contaminations. (c) AARE activity measured using AcAla-pNA is present in isolated plastid fractions and in organelle-depleted intracellular fractions. In mitochondrial fractions only weak activity is detectable. The activity is indicated by the increase of the absorbance at 410 nm (A_{410}) over time caused by the release of pNA. Mean values from technical triplicates with standard deviation are shown.
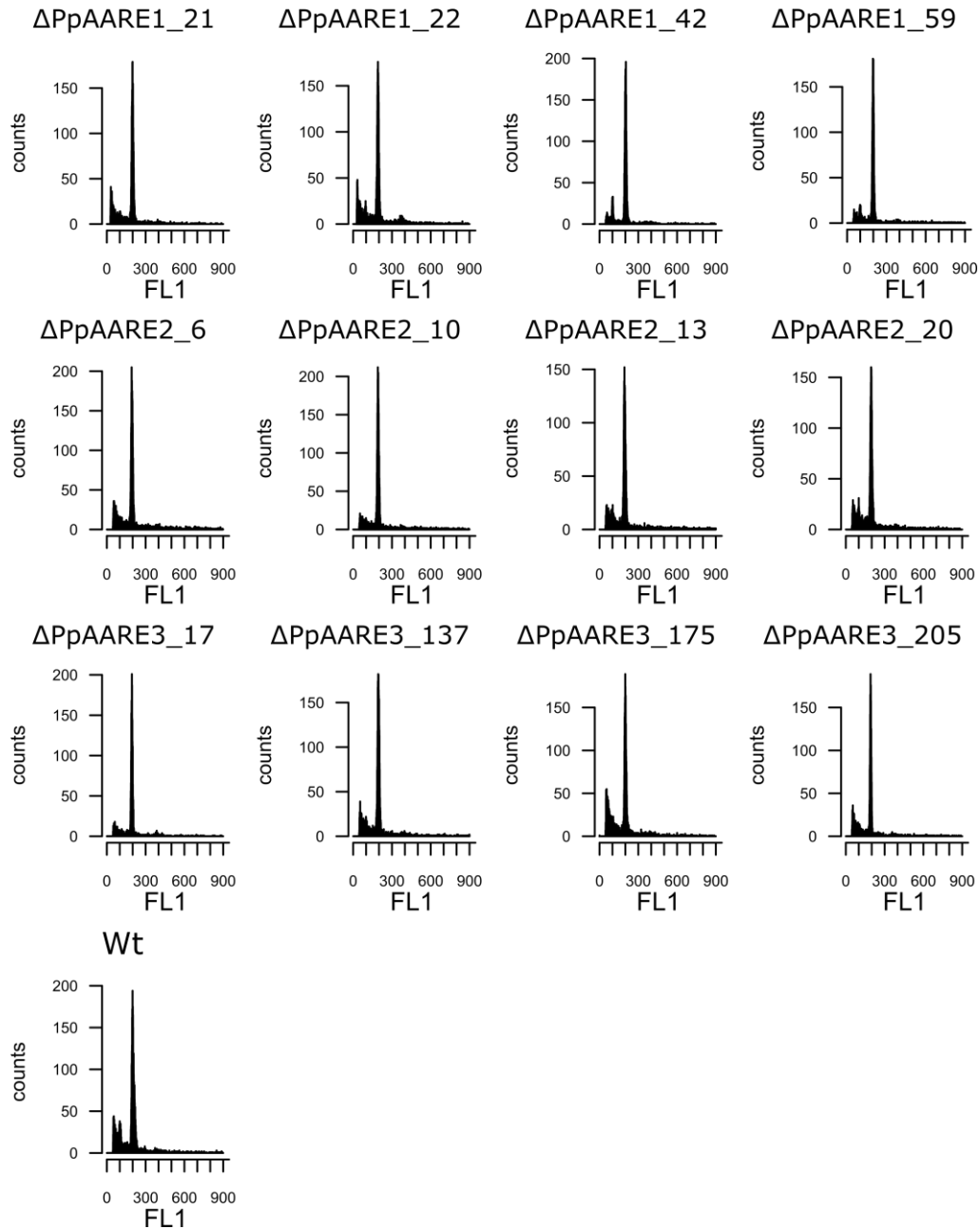
Figure S4 FCM analysis of confirmed PpAARE KO-Lines. Ploidy was determined in protonema as described in Schween et al. (2003). All lines have the major signal at ~200 like the haploid wild type.
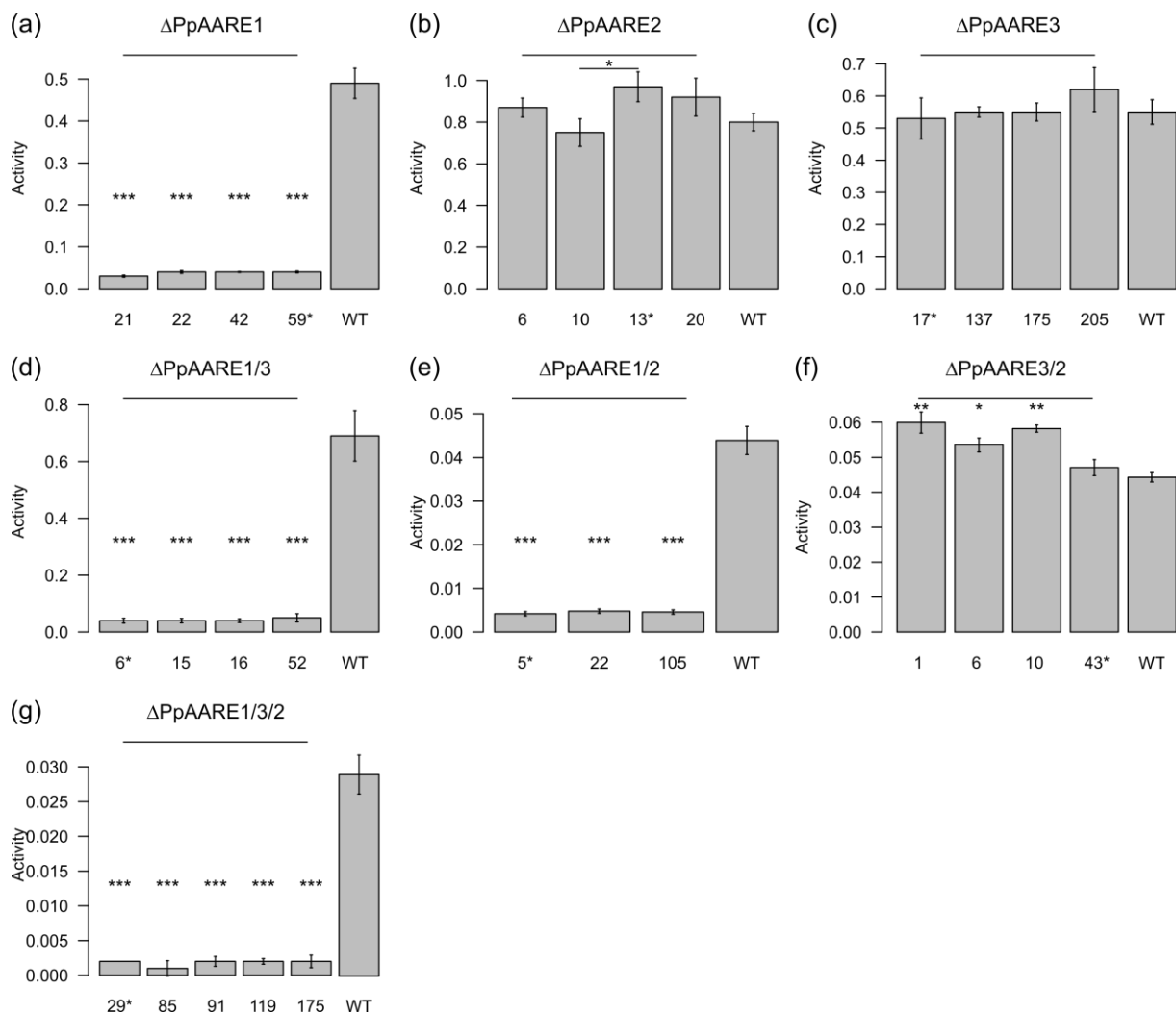
Figure S5 Mean AARE activity with standard deviations in PpAARE KO mutants. AcAla-pNA was used as substrate and activity was measured in protonema. Significance levels are based on a one-way Anova with subsequent post-hoc test (*: p<0.05, **: p>0.01, ***: p<0.001) and indicate the difference compared to the wild type (WT). All lines with a knockout of PpAARE1 have significantly reduced activity (a, d, e, and g). The mean activity of ΔPpAARE2 line 10 is significantly lower when compared to activity of ΔPpAARE2 line 13 but the activity of the latter line does not significantly differ from WT (b). The mean activity is not reduced in ΔPpAARE3 lines (c). The double knockout of PpAARE3/2 results in a significant increase of activity (f). Stars at the line numbers indicate the lines with only a single copy of the respective knockout construct which were used for the further experiments in this study.
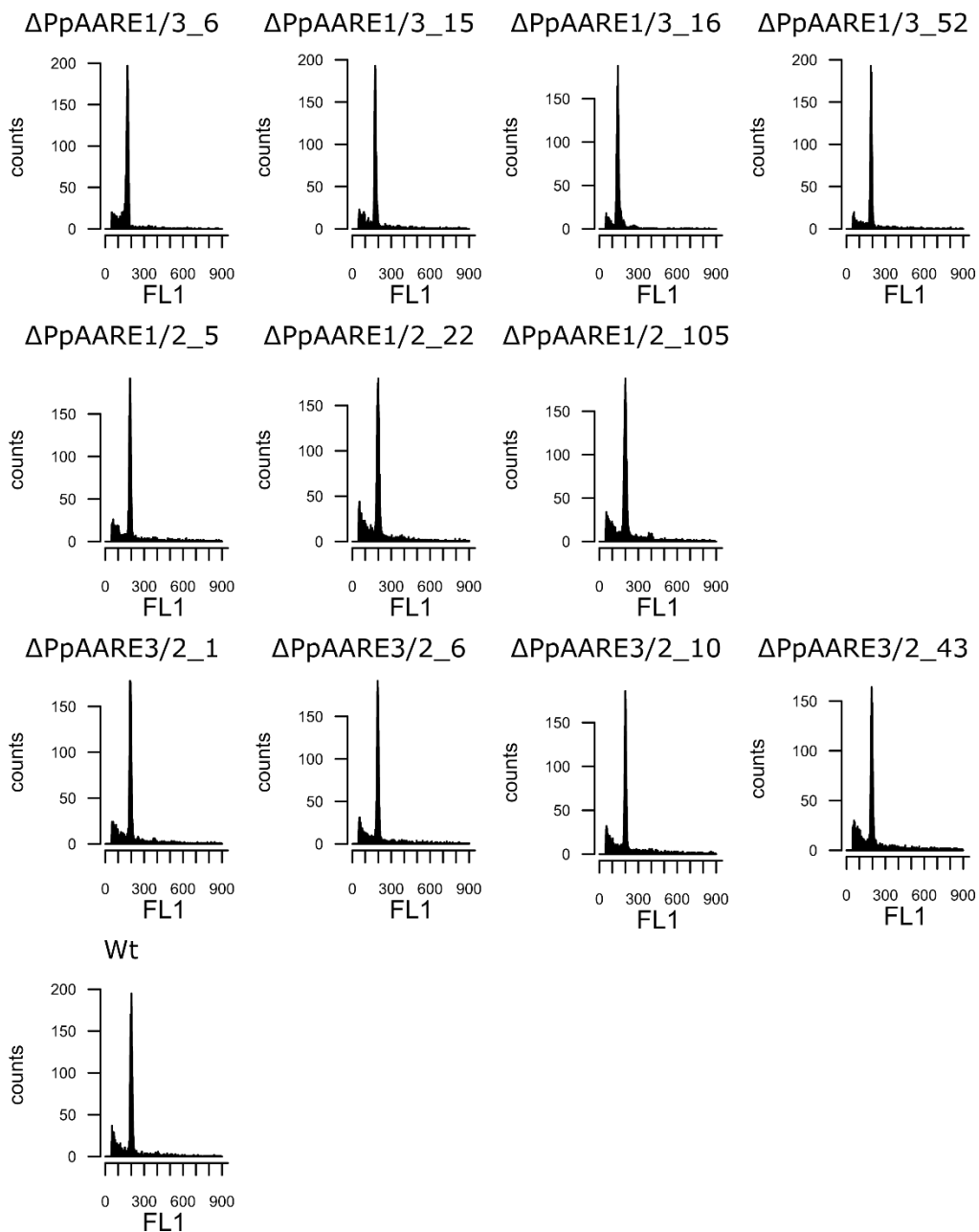
Figure S6 FCM analysis of confirmed PpAARE double KO-Lines. Ploidy was determined in protonema as described in Schween et al. (2003). All lines have the major signal at ~200 like the haploid wild type.
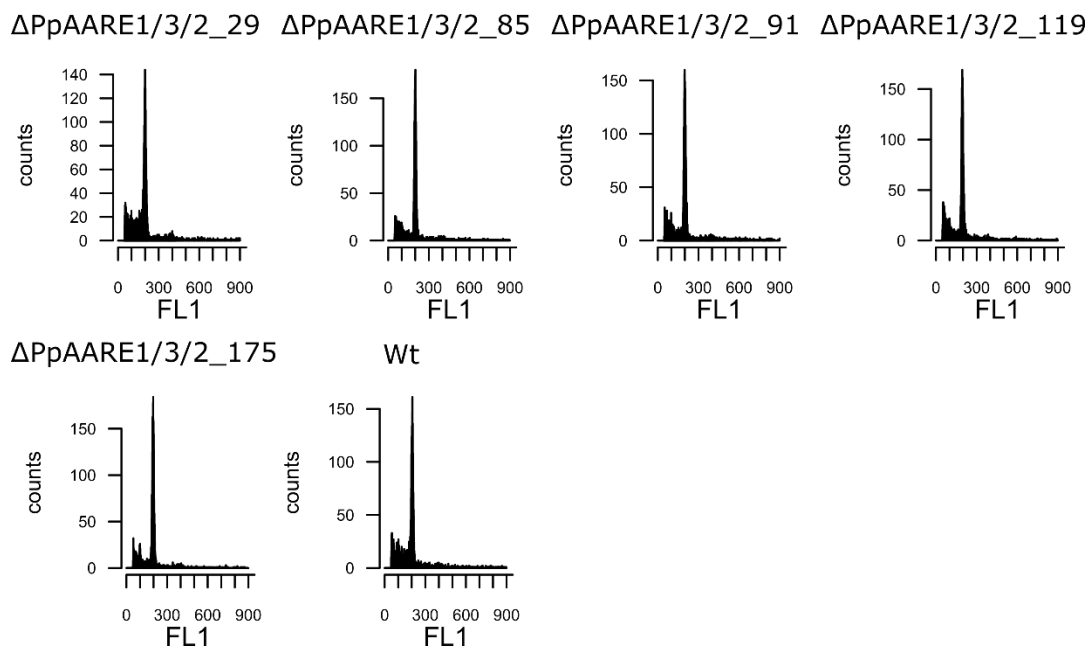
Figure S7 FCM analysis of confirmed PpAARE triple KO-Lines. Ploidy was determined in protonema as described in Schween et al. (2003). All lines have the major signal at ~200 like the haploid wild type. All double knockout lines are haploid.
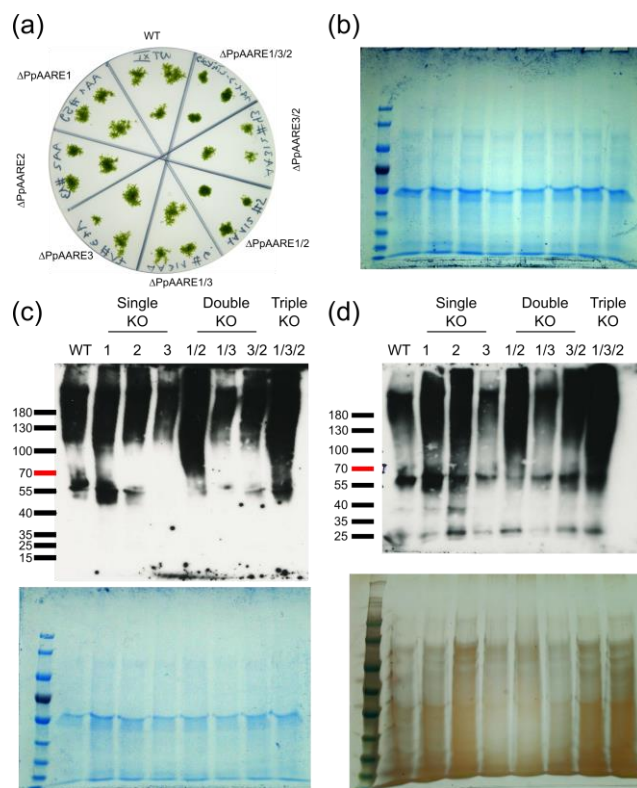
Figure S8 Plate overview and additional OxyBlots from Physcomitrella gametophore colonies with loading controls. (a) Exemplary plate (KnopME) with five-week-old gametophore colonies from WT, single, double and triple knockouts. Protein extracts from single colonies were used for OxyBlot analysis. (b) Coomassie-stained loading control for the OxyBlot depicted in Fig. 8. (c+d) Additional OxyBlots with Coomassie- (c) and silver-stained (d) loading controls. Equal volumes from the same derivatized protein solutions were loaded for the OxyBlot as well as for the loading control gels. PageRuler™ Prestained Protein Ladder (Thermo Scientific™, #26166) was used for all Blots and loading control gels. OxyBlot analysis was performed with the OxyBlot™ *Protein Oxidation Detection Kit* (Merck) according to the manufacturer's instructions.
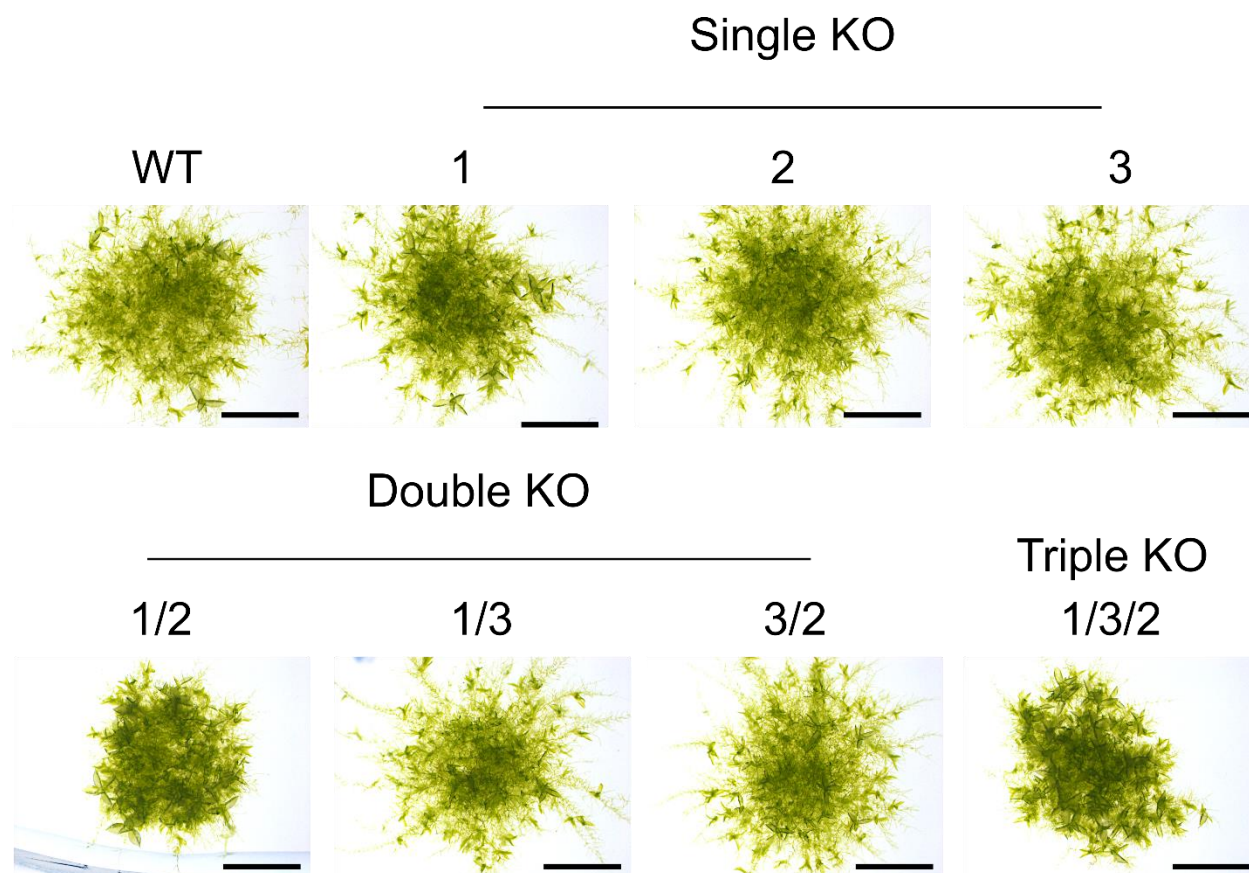
Single KO

WT   1   2   3

Double KO

Triple KO

1/2   1/3   3/2   1/3/2

Figure S9 16-day old Physcomitrella colonies. 15 µL droplets of protonema suspension cultivated under standard conditions were spotted on KnopME plates with 0.02% glucose. Colonies of the double KO PpAARE1/2 and the triple KO have more and bigger gametophores. Bar = 1 mm.
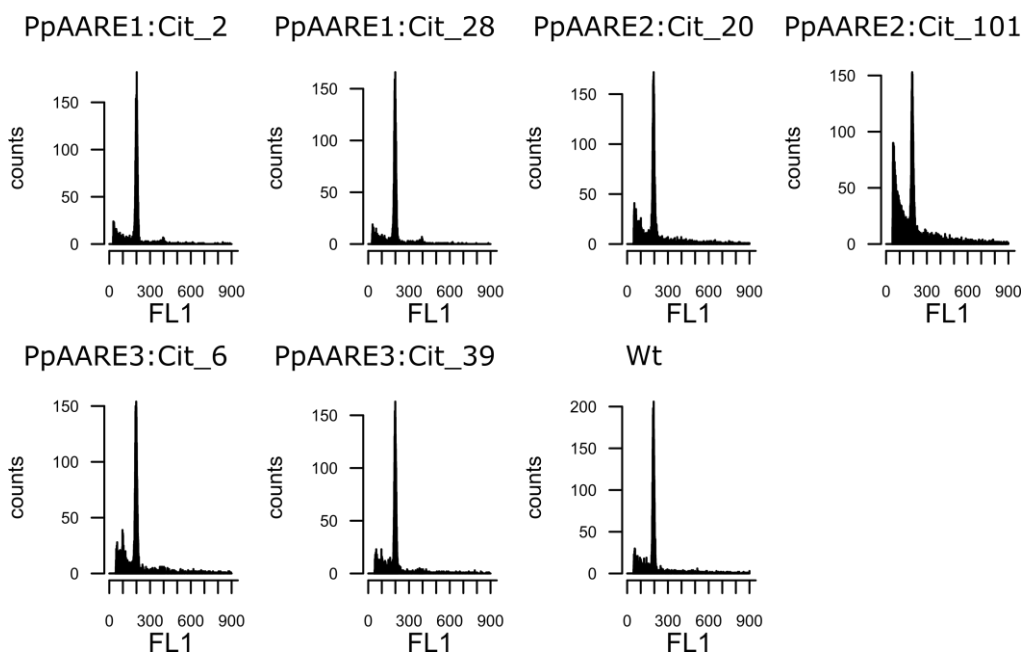
66

Figure S10 FCM analysis of confirmed PpAARE:Citrine fusion lines. Ploidy was determined in protonema as described in Schween et al. (2003). All lines have the major signal at ~200 like the haploid wild type. All double knockout lines are haploid.
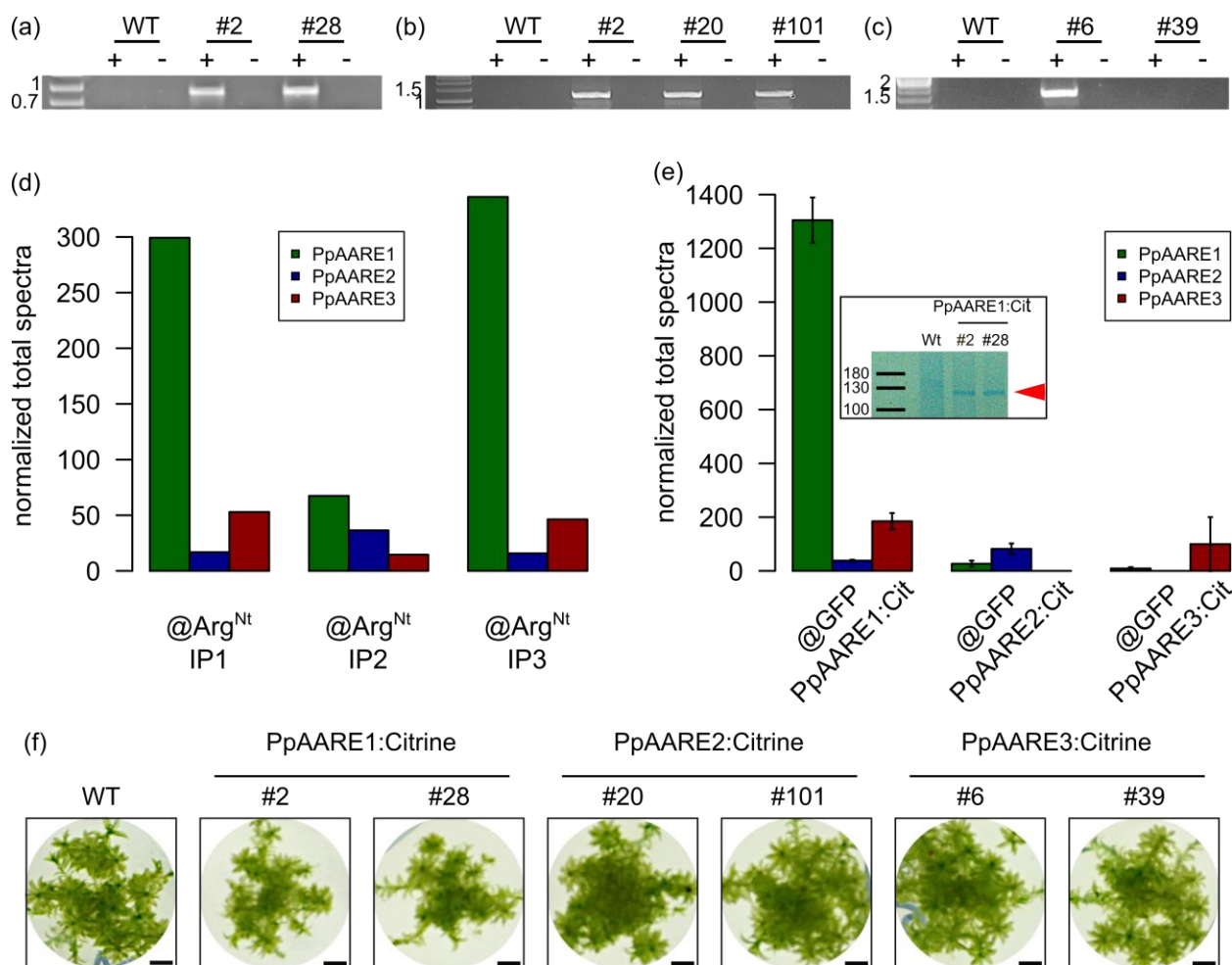
Figure S11 Screening for Physcomitrella lines with a citrine fusion transcript and overview on identification of the three PpAARE isoforms in different IP experiments. (a)-(c): RT PCR on citrine fusion candidate lines for PpAARE1 (a), PpAARE2 (b), and PpAARE3 (c). +: with cDNA template; -: without reverse transcriptase. For each PCR a forward primer binding in the CDS of the respective PpAARE isoform and a reverse primer binding in the CDS of citrine was chosen. Primers are listed in Table S2. No transcript was detected in PpAARE3:Citrine #6. PpAARE2:Citrine #2 was not used for further experiments. (d) All PpAARE isoforms were identified in the IP experiments targeting N-terminal arginylation (Hoernstein et al., 2016). Identified proteins are listed in Table S7. Details of the database search are specified in the supplemental procedures. (e) Overview on identification of PpAARE isoforms in the test IP experiments targeting the citrine tag of the different fusion proteins. The test IP against PpAARE1:Citrine was performed using *Dynabeeds M270 Epoxy Co-Immunoprecipitation Kit* (Life Technologies, Carlsbad, USA) with a monoclonal anti-GFP antibody (Roche, REF

11 814 460 001) as described in for two independent fusion lines (#2 and #28). Eluted proteins were separated via SDS-PAGE and bands (inset, red arrow) corresponding to the expected size (112 kDa) were excised and analyzed by mass spectrometry. Test IP experiments against citrine-tagged PpAARE2 and PpAARE3 were performed with GFP-Trap Magnetic Particles (Chromotek) followed by an on-bead digestion with trypsin and subsequent mass spectrometry. Bars represent mean values with standard deviation of normalized total spectra obtained in each two independent fusion lines (PpAAR2: #20, #101; PpAARE3: #6, #39). (f) Gametophore colonies of selected Citrine fusion lines cultivated 4 months on solid medium. Bar = 2 mm.
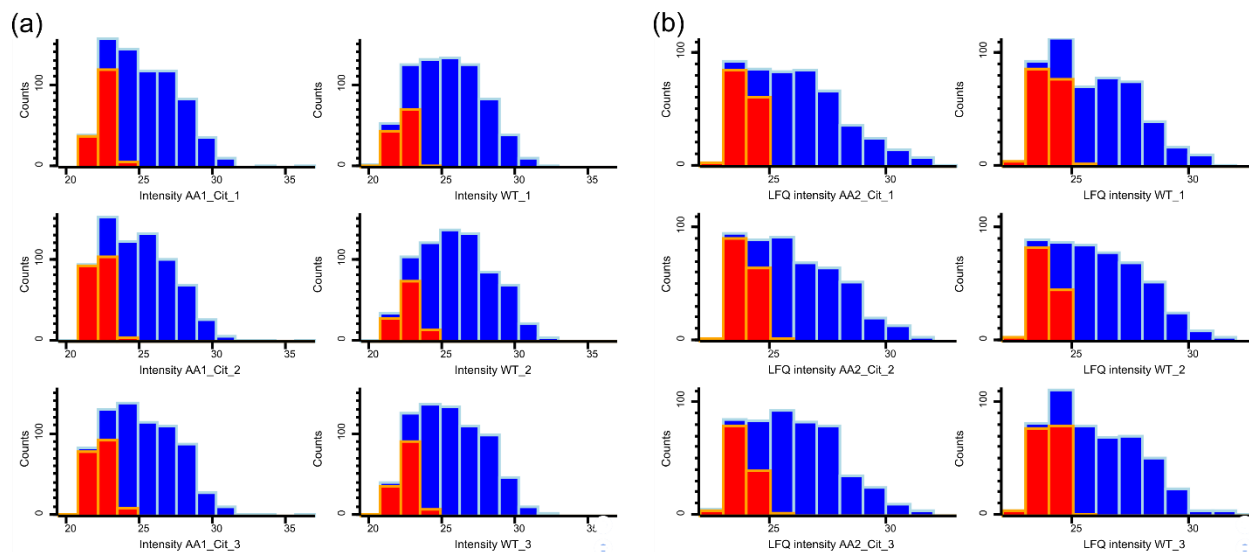
Figure S12 Histograms of label free quantitation (LFQ) intensities from MaxQuant software used for interaction analysis. Blue bars represent experimentally observed LFQ intensities. Red bars represent missing values imputed with Perseus Software. (a) Co-IP on PpAARE1:Citrine. (b) Co-IP on PpAARE2:Citrine.
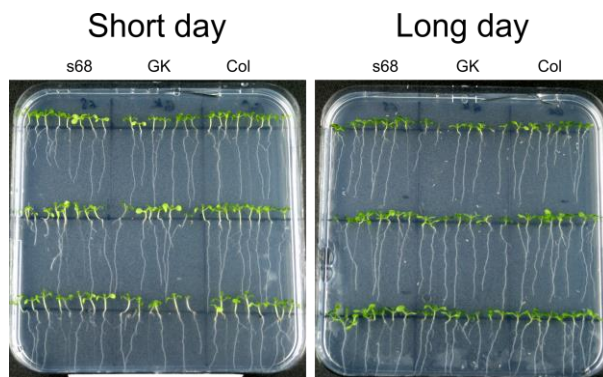
Figure S13 AtAARE T-DNA mutant lines (GK, s68) and WT (Col) grown in short- or long-day conditions. Short day: 8h light /16h dark, 35 µmol/m^{2}s; Long day: 16h light / 8h dark, 35 µmol/m^{-2}s. No obvious differences of the phenotype are observable between seedlings of mutant lines (s68, GK) and WT (Col).

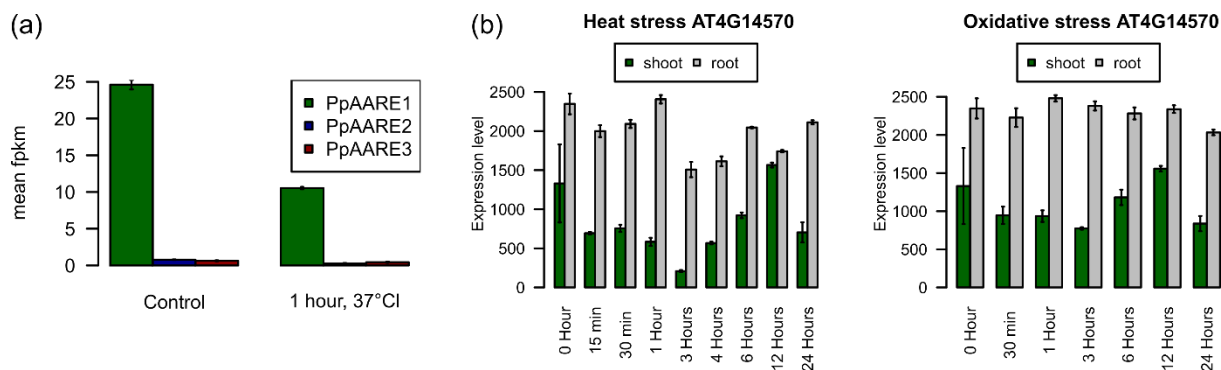**Figure S14** Expression data for AARE isoforms in Physcomitrella and Arabidopsis in response to heat and oxidative stress. (a) Expression levels for PpAARE1, PpAARE2 and PpAARE3. Data were downloaded from PEATmoss (https://peatmoss.online.uni-marburg.de/) and described in Perroud et al. (2018) and Fernandez-Pozo et al. (2020). (b) Expression levels of AtAARE. Data were downloaded from the Arabidopsis eFP Browser (http://bar.utoronto.ca/efp_arabidopsis/) and described in Kilian et al. (2007) and Winter et al. (2007).

71

Supplemental methods:

AARE activity in plant tissues

The enzyme activity assay was modified after Yamauchi et al. (2003). In brief, tissue (80-100 mg) was homogenized in liquid nitrogen and dissolved in 1 mL extraction buffer (50 mM PBS, 1 mM EDTA, 2 mM DTT). After centrifugation at 20,000 x g for 20 min at 4°C, 300 µl supernatant was mixed with 700 µL reaction buffer (50 mM HEPES-KOH, pH 7.5 containing 1 mM Ac-Ala-pNA (Bachem, Bubendorf, Switzerland) or 50 mM HEPES-KOH, pH 7.5, 10% DMSO containing 1mM AcLeu-pNA (Bachem) and incubated at 37°C for 30-120 min. The reaction was stopped by the addition of 500 µL 30% acetic acid. Absorbance was measured at 410 nm in a photospectrometer. Activity was calculated using a molar absorbance coefficient of 8.8 mM*cm^{-1} according to Nakai et al. (2012). The reaction was performed in triplicates. The protein concentration was determined using the A_{280} method of a NanoDrop^{TM} (Thermo Fisher Scientific) or with a Bradford assay (Bradford 1976) und used for normalization of the activity. The activity in PpAARE1/2 and PpAA3/2 double knockouts was measured by mixing 5 µL protein extract with 195 µL reaction buffer in a 96 well plate. Each reaction was performed in triplicate. The absorbance values at A_{410} were recorded after 60 or 120 min and in a plate reader without stopping the reaction.

Revised database search on dataset PXD003232

Processed mgf files from immunoprecipitation experiments targeting N-terminal arginylation (Hoernstein et al., 2016, PXD003232) were searched against all Physcomitrella protein models V3.3 (Lang et al., 2018) using Mascot Server V2.7.0 (Matrix Science). The precursor mass tolerance was 5 ppm and the fragment mass tolerance was 0.02 Da. Variable modifications were formation of pyro Glu (N term Q, −17.026549 Da), oxidation (M, +15.994915 Da), acetylation (N-term, +42.010565 Da) and deamidation (N, +0.9 84016 Da). Carbamidomethylation (C, +57. 021464 Da) was specified as fixed modification. Enzymatic specificity was set to tryptic with semi-specific free N-terminus. Search results were loaded in Scaffold^{TM} 5 V5.0.1 (Proteome Software) and proteins were accepted at an FDR = 1 and peptides at an FDR = 0.5. A table of identified proteins is accessible in supplemental table S7.

Supplemental references:

Ashton NW, Grimsley NH, Cove DJ (1979) Analysis of gametophytic development in the moss, *Physcomitrella patens*, using auxin and cytokinin resistant mutants. *Planta* 144: 427-435

Fernandez-Pozo N, Haas FB, Meyberg R, Ullrich KK, Hiss M, Perroud PF, et al. (2020) PEATmoss (Physcomitrella Expression Atlas Tool): a unified gene expression atlas for the model plant *Physcomitrella patens*. *Plant Journal* 102: 165-177

Hoernstein SNW, Mueller SJ, Fiedler K, Schuelke M, Vanselow JT, Schuessele C, et al. (2016) Identification of targets and interaction partners of arginyl-tRNA protein transferase in the moss *Physcomitrella patens*. *Molecular & Cellular Proteomics* 15: 1808-1822

Kilian J, Whitehead D, Horak J, Wanke D, Weinl S, Batistic O, et al. (2007) The AtGenExpress global stress expression data set: protocols, evaluation and model data analysis of UV-B light, drought and cold stress responses. *Plant Journal* 50: 347-363

Lang EGE, Mueller SJ, Hoernstein SNW, Porankiewicz-Asplund J, Vervliet-Scheebaum M, Reski R (2011) Simultaneous isolation of pure and intact chloroplasts and mitochondria from moss as the basis for sub-cellular proteomics. *Plant Cell Reports* 30: 205–215

Lang D, Ullrich KK, Murat F, Fuchs J, Jenkins J, Haas FB, et al. (2018) The *Physcomitrella patens* chromosome-scale assembly reveals moss genome structure and evolution. *Plant Journal* 93: 515-533

Mergner J, Frejno M, List M, Papacek M, Chen X, Chaudhary A, et al. (2020) Mass-spectrometry-based draft of the Arabidopsis proteome. *Nature* 579: 409-414

Notredame C, Higgins DG, Heringa J (2000) T-Coffee: A novel method for fast and accurate multiple sequence alignment. *Journal of Molecular Biology* 302: 205-217

Perroud PF, Haas FB, Hiss M, Ullrich KK, Alboresi A, Amirebrahimi M, et al. (2018) The *Physcomitrella patens* gene atlas project: large-scale RNA-seq based expression data. *Plant Journal* 95: 168-182

Schween G, Gorr G, Hohe A, Reski R (2003) Unique tissue-specific cell cycle in *Physcomitrella*. *Plant Biology* 5: 50–58

Waterhouse AM, Procter JB, Martin DM, Clamp M, Barton GJ (2009) Jalview Version 2—a multiple sequence alignment editor and analysis workbench. *Bioinformatics* 25: 1189-1191

Winter D, Vinegar B, Nahal H, Ammar R, Wilson GV, Provart NJ (2007) An "Electronic Fluorescent Pictograph" browser for exploring and analyzing large-scale biological data sets. *PLOS ONE* 2: e718

Yamauchi Y, Ejiri Y, Toyoda Y, Tanaka K (2003) Identification and biochemical characterization of plant acylamino acid–releasing enzyme. *Journal of Biochemistry* 134: 251-257